Development of MoS_2-ZnO Heterostructures: An efficient Bifunctional Catalyst for the Detection of Glucose and Degradation of Toxic Organic Dyes

By

Farhan Ali

School of Chemical and Materials Engineering (SCME)

National University of Sciences and Technology (NUST)

June, 2022

Development of MoS_2-ZnO Heterostructures: An efficient Bifunctional Catalyst for the Detection of Glucose and Degradation of Toxic Organic Dyes

Farhan Ali

Reg No. 00000274234

This thesis is submitted as a partial fulfillment of the requirements for the degree of

Master of Science in Nano science and Engineering

Supervisor Name: Dr. Sofia Javed

School of Chemical and Materials Engineering (SCME)

National University of Sciences and Technology (NUST)

H-12 Islamabad, Pakistan

June,2022

DEDICATIONS

With deep sense of gratitude, humbleness, and warmest affection I would like to dedicate this thesis to my family and colleagues for their continuous help and support.

ACKNOWLEDGEMENT

All praise and gratitude belong to Allah Almighty for giving me the strength, ability, and opportunity to understand, learn and complete this research work.

Special appreciation goes to my research supervisor Dr. Sofia javed and Dr. Mashkoor Ahmed for their precious time and constant support throughout my work. This research could not have been possible without his invaluable guidance, constructive comments, and suggestions throughout the experimental and thesis work.

I am also thankful to my family, friends and colleagues for their moral support, kindness, and care. Thank you all very much.

Farhan Ali

Reg No. 00000274234

Abstract

Synthesis, Characterizations of Molybdenum disulfide& Zinc oxide for Photo catalysis & bio sensing application is reported in this work. The material was synthesized using two step hydrothermal route from Sodium Molybdate, Sulfur, Hydrazine, Ammonia & Zinc Nitrate hexa-hydrate. In first step molybdenum disulfide is synthesized. The reaction temperature was 150^{o}C. The time of reaction was 34 hrs. The resultant was then washed & dried to obtain MoS_2 in form of shimmery black powder, In second step MoS_2.ZnO is synthesized the reaction temperature was 80^{o}C. The time of reaction was 6 hrs.

X-Ray studies confirmed the formation of crystalline MoS_2.ZnO. The SEM of sample confirms the flower-like morphology of the sample. The TEM image reveals that sample is consist in of spherical particles, Nano flowers and rod like structures. The EDX results are also in good agreement with the stoichiometric values of the chemicals used. Finally study regarding the Bio sensing and photo catalytic applications has been conducted to check out the sensitivity and catalytic activity of molybdenum disulfide/Zinc Oxide Nano composite. For this purpose experiments for non-enzymatic detection of glucose has been performed through 3-electrode based system. First, CV curves for the different concentration of glucose in pH 7.0 PB solution are recorded and analyzed without using any enzyme. Results have shown a good relation between peak current and concentration of glucose in range of 50 µm and 5000 µm. So, effective sensitivity, large surface area and high electrical conductivity made Nanostructure of MoS_2/ZnO a promising material for bio sensing. in second phase MoS_2/ZnO electrode has been tested for degradation of organic dyes like MB, RHB , Sandoz Yellow etc. due to good optical properties of ZnO and band gap tuning using MoS_2 the large range of light is harvested which increase the degradation rate of organic dyes as shown in degradation graphs.

Table of Contents

Table of Figures

List of Tables

Chapter 1

Introduction

Nanotechnology deals with the study of Nanostructures and Nanomaterials and their physical properties which uses the design fabrication technology [1, 21]. It describes the association between the physical properties and material dimensions in Nano scale. According to the United States definition, Nanoscale is the unit which measures the materials and systems structures and components which play role in their unique and notably better physical, chemical, and biological properties, phenomena and processes defined as nanotechnology [3]. Generally, in micrometer scale, materials show the same physical properties as that of bulk but in Nano scale materials show different physically properties than that of bulk. Nanomaterial displays extraordinary properties for example, low melting point and reduced lattice constant has been reported in the Nanometer crystals [4]. Surface atoms or ions has huge impact in the total numbers of atoms or ions while the surface energy count for thermal stability. Nanoscale range also plays important role in Crystal structures stability at different temperature ranges. Therefore, Ferroelectric and ferromagnetic material might miss out their electricity and magnetism when they are in Nanometer range. When the characteristics feature of bulk semiconductor is lie in Nanometer range, they become insulator [4]. The bulk gold does not show any catalytic properties while the Au Nano-crystal exhibits remarkable low temperature catalyst effect. Several dimensions are used to classify Nanomaterial's, which are not restrict to the Nano scale (<100 nm) are Zero-dimensional (0-D) one-dimensional (1-D) two-dimensional (2-D) and three-dimensional (3-D). Those materials which exhibit all the dimensions in the Nano scale (no dimensions, or 0-D) are called zero Nanoparticles quantum dots. Nanowires are the most common representation of zero-dimensional Nanomaterial's. One-dimension material includes Nanotubes, Nano rods and 16 dimensional material. 2-D materials

exhibit two dimensions in the other scale and present planar shapes including Nano films, Nano layers, Nano coatings. Whereas nanoscale is not used to measure the Bulk Nanomaterial in any dimension. These materials are thus characterized on the basis of three random `dimensions given above 100 nm. These three dimensional Materials either have a Nano crystalline structure or show the features at the Nano scale. Concerning the Nano crystalline structure, multiple Nano size crystals are arranged in layers in bulk Nanomaterial's in different orientations. Those features present at the Nano Scale, shows the 3-D Nanomaterial which contains scattered Nanoparticles, roll of Nanowires and Nanotubes as well as several Nano layers [5]. When Nanomaterial's and Nanostructures processed and fabricate , it's important to control the huge surface energy, which is the outcome of large surface area or extensive surface to volume ratio. The Nanomaterial's should be designed with uniform size distribution, crystallinity, microstructure, morphology, and chemical composition to get desired physical properties we have to prevent Nanostructures and Nanomaterial's from agglomeration as a time evolves [4]. Glucose sensors used in diagnostics in clinical setup, in inspection of food and biotechnology which urge the need to develop the fast, sensitive and reliable glucose sensor. To date, Electrochemical sensors proved to be advantageous due to the high sensitivity, time efficiency, basic instrumentation, effortless operation, and cost-effectiveness. For this reason, they are invariably recognized as the most appropriate and constructive tool for glucose analysis [81,82]. Glucose oxidase (GOx) and non-enzymatic materials modified sensors used the electrochemical method which is extensively studied. GOx activity is more vulnerable to meteorological factors in contrast to non-enzymatic sensors [83]. It is the good substitute of enzymes which due to their high cost and demand of non-physiological electron mediators or oxygen becomes ineffective [84]. Non-enzymatic glucose sensors now the prime concern to many industries as it also possess the various metal Nanoparticles [85–86]. Industrial effluent commonly discharged into wastewater which not only affects the water quality but also disturb the life under water by hinder the sunlight infiltration into the water and significantly reduced the sea food chain. Besides many dyes reported as damaging and capable of introducing the carcinogenic properties [87, 88]. Now a days waste water contains the different heavy metals which cannot be treated through conventional

wastewater treatment methods [89]. Modern methods include the various chemical and physical processes, in which activated carbon are used on which the waste water components get adsorbed. Besides this, other processes such as coagulation through chemical agent, hypochlorite oxidation, ozone oxidation, and electrochemical method, etc. also used to treat the wastewater effluents containing dyes. These methods are the source which produce the secondary waste products. However, its cost and inefficiency made it less reliable [90]. In this technology era, innovative methods which are environment friendly as well as cost effective and efficient need to be investigate. In recent years, semiconductor materials are highly utilized due to their capability to oxidize the organic compounds through photocatalytic process which can be used as an substitute to conventional methods for the removal of resistant organic pollutants from water. In this process, water molecule or hydroxyl group interact with the valance band holes generated by UV photons and adsorbed on the catalyst surface and give rise hydroxyl radical (•OH), or electron in the conduction band. When these hydroxyl radical interact with adsorbed oxygen molecule, it forms the oxygen radical $\bullet O_2^-$ and hydroperoxyl radical •OOH radicals. The in situ formation of these radicals made them highly reactive and unselective oxidants [91–92]. ZnO and TiO2 are the upmost semiconductors which have been used as photocatalyst due to their high photocatalytic activity, non-toxic nature, inexpensive, and excellent chemical and mechanical stability.

When ZnO and TiO has been compared, TiO2 is commonly used as the most active photo catalyst. However as both ZnO and TiO has the same band gap energy around 3.2 eV ,ZnO can also be used in place of TiO2 as it works effectively in both acidic and basic environment with the high degradation capability of organic components. These properties led to many researchers to investigate the ZnO properties which could help in many photocatalytic reactions. [93–94]

1.1 Molybdenum Disulfide (MoS2)

Molybdenumdisulfide belongs to the family of layered transition metal dichalcogenides. It occurs as a mineral called “molybdenite” and this inorganic compound exhibits shiny

silver black color in visible range. It usually appears as graphite and it is not highly reactive molybdenum disulfide contains an interlayer structure in which molybdenum layer is embedded between upper and lower layer of Sulfur. Vander Walls Forces loosely bound the layers of Mo and Sulfur to one another in Molybdenum disulfide. These Vander walls Forces are responsible for easy cleavage of S-MO-S direction in (001).

On the basis of XRD pattern, the following three type of ill-Crystallized MoS_2 exist

i. **Amorphous**
ii. **Single layered**
iii. **Poorly Crystalline**

On the basis of 002 and 110 diffraction planes in their XRD patterns Chinealli et al. has differentiated between the amorphous MoS_2 and poorly crystalline MoS_2. These two type of MoS_2 usually distinguished from Crystalline MoS_2 in catalytic and electrochemical properties. It is also observed that these properties varies inversely when it comes to crystallinity of MoS_2.

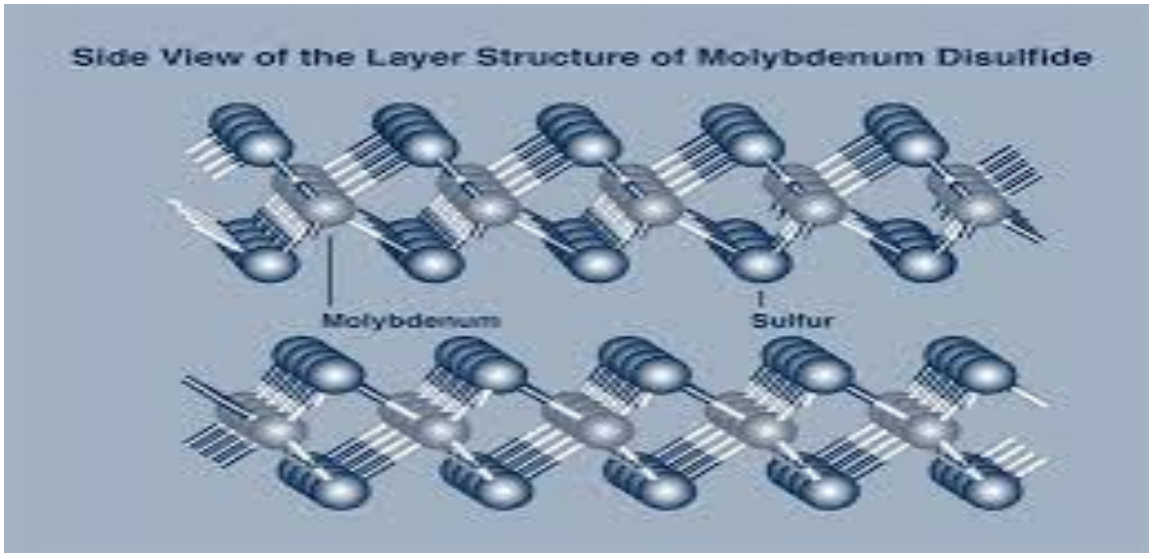

Figure 0-1Crystal structure of MoS2

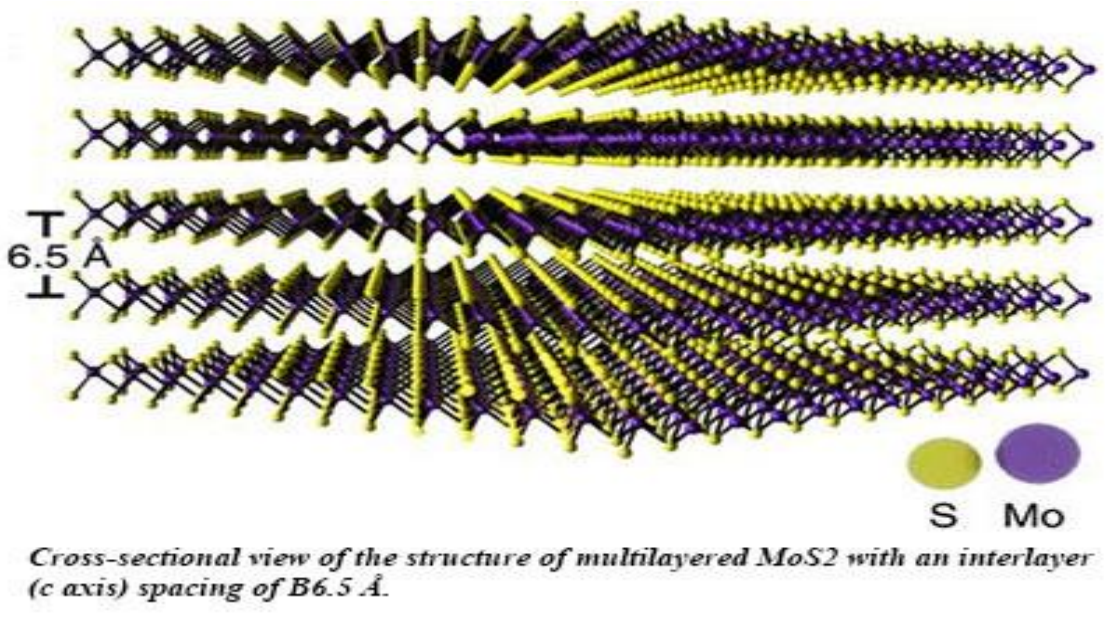

Figure 0-2Crystal structure of MoS2

The thickness of as prepared monolayer of molybdenum disulfide is 6.5A while bilayer molybdenum disulfide thickness is calculated as 13A. The thickness of single layer MoS_2 is almost the half of bilayer MoS_2. Molybdenum disulfide is a semiconductor of direct band gap with 1.23-1.69 eV band gap energies. When dimensions are reduced from bulk structure to 2-Dimension monolayer structure, the indirect band gap of molybdenum disulfide bends to the direct band. The apparent qausi particle band gap for molybdenum disulfide is calculated to be 2.40 ± 0.05 eV for single layer, 2.10 ± 0.05 eV for bilayer and 1.75± 0.05 eV for tri-layer molybdenum di sulfide. Molybdenum disulfide exhibits the unexpected band gap tune ability (as large as 0.85 ± 0.05 eV) is single layer molybdenum disulfide which depends upon grain boundary mis-orientation angle.

1.1.1 Structure of MoS_2

All forms of molybdenum disulfide has a various layer structure in which planes of molybdenum are embedded between planes of sulfur oriented in (001) plane direction. Molybdenum ion and Sulfur ion are attached to each other by a Covalent Bond. These three strata form a monolayer of molybdenum disulfide. Weak Vander Walls forces bind them together in bulk form. Naturally crystalline MoS_2 exists in rhombohedral and

hexagonal symmetry and are represented by 2H- MoS_2 and 3R- MoS_2, where H and R represents hexagonal and rhombohedral symmetry respectively. Molybdenum acquire the center of trigonal prismatic coordination sphere in both hexagonal and rhombohedral structures and is covalently bonded to sic sulfide ions. The lattice constants of molybdenum disulfide are measured to be a=0.3161nm b= 0.3163 nm (3R) c= 1.2295 nm.

1.1.2 Methods of synthesis

Numerous methods are reported for the synthesis of Nanomaterials, it has been realized that crystal allotropic structure is central importance while synthesizing low dimensional Nano materials. However, MoS_2 can be synthesized at higher temperature (800-900) as mono or poly crystalline material or at low temperature through chemical route. Some of physical properties of said material can be controlled by following synthesis at low temperature. So far MoS_2 Nano-particles have been synthesized by using the below mentioned methods

1. Hydrothermal
2. Solvothermal
3. Inverse micelle method

1.1.3 Solvothermal method

This method is combination of solvo and thermal methods. Solvothermal is a procedure used for preparation of compounds and chemicals in which non-aqueous precursor are used. We can control the shape, size distribution and crystallinity of Nano structure by controlling the temperature of reaction, type of reaction, type of precursor and pressure etc. Solvothermal method serves as a low temperature approach for synthesis of molybdenum disulfide, Molybdenum trioxide and Sulfur are usually used as starting agents for synthesis of molybdenum disulfide in presence of reducing agent at a temperature around 300C. Molybdenum disulfide produced by this method usually have hollow sphere symmetry but in the excess presence of Sulfur contents resulting material obtains possess crystalline symmetry.

1.1.4 Inverse micelle method

In this method micelles are dispersed in non-aqueous media in which particles are grown. The major precursor usually used are molybdenum halide and sulfiding agent. By controlling the size of micelle one can control the size of particles. The size of micelle is dependent upon ratio of emulsifier and water. The ratio of emulsifier to water is usually altered to vary the size of micelle and in turn to get the desired size of particle. Particle size up to 2.5 nm can be achieved by inverse micelle method. However instability of molybdenum halide has limited the efficiency of this method in production of molybdenum disulfide. Never the less this method is considered best for the synthesis of other type of semiconducting Nano-particles.

1.1.5 Hydrothermal Method

In hydrothermal method particles are grown in an aqueous solvent at a temperature higher than room temperature while one bar high pressure. Nano crystalline materials under low temperature can be effectively grown through this method without further annealing. Precursor solution is maintained in autoclave at a temperature ranges between 100-300 C over the period of time. MoS_2 synthesized from this method has shown increase catalytic activity during hydrogen evolution reaction. The reactions conditions like temperature, pressure, type of precursor and reaction time effects the size plus morphology of the final product. In this research hydrothermal method is used for synthesis with specific reaction condition to get control over final product.

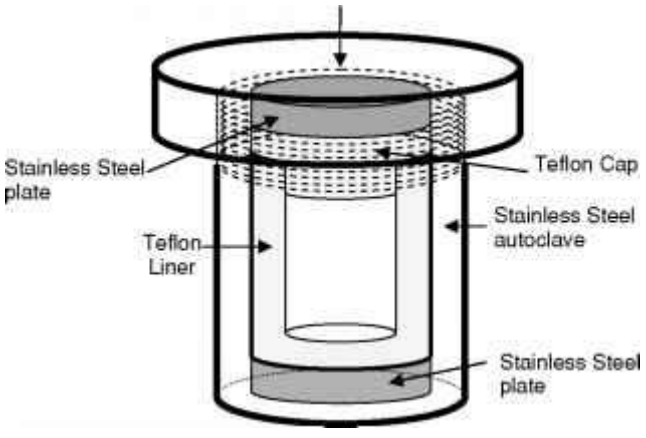

Figure 0-3Auto Clave

Some other methods:

Some other methods we found in literature for the synthesis of MoS_2 are as follows

1. Sonolysis
2. Plasma microwave
3. Electrochemical / Chemical method
4. Chemical Vapor deposition method
5. Chemical Exfoliation

1.2 Molybdenum Disulfide as a Biosensor

2D MoS_2 possesses some remarkable properties that are adventurous for its bio sensing application. Especially when grown with large lateral dimension, basal planes of Molybdenum disulfide have no dangling bonds than they can be efficiently incorporated into bio sensing structures due to their stability in liquid and oxygen containing gaseous media. The bio sensing performance of molybdenum di sulfide can be enhanced by creating substantial surface to volume ratio of the material. The suitable band gap increases the sensitivity of the material based on 2D Molybdenum disulfide than that of small or zero band gap graphene and graphene oxides. The whole thickness of MoS_2 get affected upon interaction with the bio molecule. To promote the specific chemical reaction on the surface of molybdenum disulfide different functionalization methods can be utilized which enable the bio sensing capability. One can transform molybdenum disulfide from semi-conducting to fully conducting by adjusting the electronic energy states which this material eligible for many bio-sensing conditions.

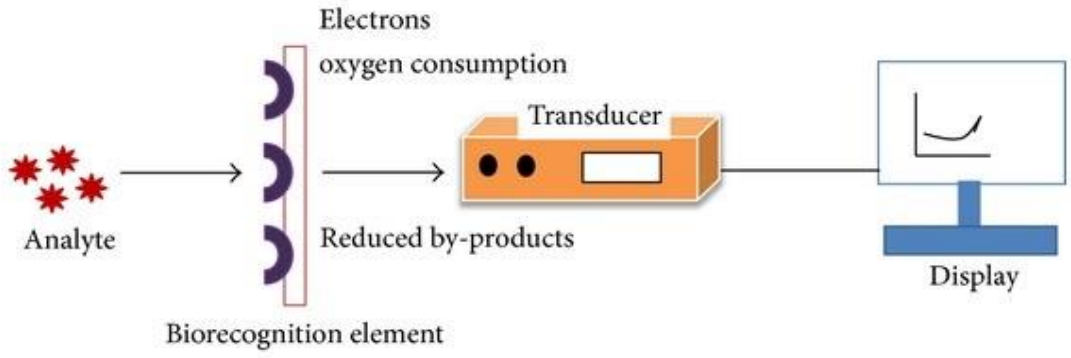

Figure 0-4Schematic diagram of Biosensor

1.3 Zinc oxide

Zinc oxide is a distinctive material which exhibit several semiconducting piezoelectric and pyro electric properties. Zinc oxide have been a part of many enzymes, sun screens, pain and itch relieving Gels. It exhibits the wide band gap which helps its microcrystal to absorb light in UVA and UVB spectral region. Zinc oxide are most effective against microorganism and works on biological functions largely depending on its morphology, particle size, exposure time, concentration, PH and biocompatibility. Zinc Oxide Nano-structures are widely used for the manufacturing of systematic amperometric bio-sensor as they present the unnatural and versatile properties including bio compatibility, non-toxicity, chemical and photochemical stability, high specific surface area, optical transparency , electrochemical activities, high electron communicating features and so on. ZnO NP's are excellent drug carrier systems.

1.3.1 Zinc oxide structure:

Wurtzite zinc oxide consists of a hexagonal structure, with tetrahedral centers O^{2-} and Zn^{2+} ions, with cubic lattice structure and parameters a=0.3296 and c= 0.52065 nm (Figure 1). The mechanical properties of wurtzite ZnO include piezoelectricity and pyro electricity. The polarization, owing to the positive charge of Zn-(0001) and negative charge of O-(0001) surfaces, of zinc oxide, along the c-axis, is another important characteristic. In order to maintain the stability of wurtzite structure, the polar surfaces and planes have surface reconstructions except in the case of zinc oxide, whereby, the

structures are flat and devoid of reconstructions. This exceptional behavior is an indication to the superior stability of wurtzite ZnO+(0001) polar surfaces. Other important facets include non-polar ZnO {$21\bar{1}0\bar{}$} and {$0110\bar{}$}.

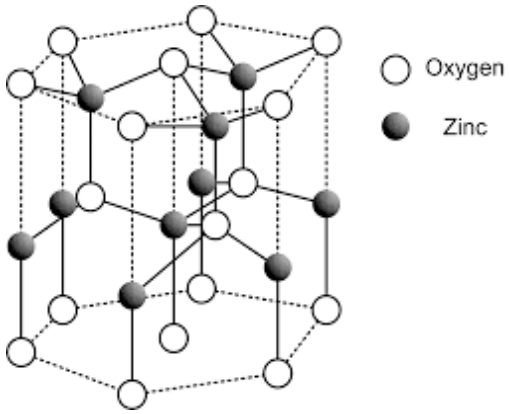

Figure 0-5Crystal structure of Zinc oxide

1.4 Properties of ZnO

The ZnO structure can be utilized in the form of chemical bulk or a semi-conductor depending on its application, owing to its optical, electrical and thermal properties. For instance, it can be used as an electrical conductor due to its thermal stability at very high temperatures i.e. 1800 °C and as a semi-conductor in opto-electronics and transparent conducting films. It has also proven to be useful in pigment applications and as an additive in rubber, owing to its high refractive index (1.95-2.10) and physical and chemical properties. It is used in desulfurization process in chemical plants due to the specific surface area of ZnO active grades. It is of utmost importance to study the various properties of ZnO structure in order for selection of material can be carried out appropriately.

1.4.1 Crystal structures

The crystallized structures of ZnO include hexagonal wurtzite, cubic zinc-blende and cubic rock-salt (NaCl-like) structures. Amongst these, the wurtzite ZnO structure is the most stable structure in terms of thermodynamically at ambient temperature and conditions. The cubic zinc-blende structure can only be stabilized when it has been

grown epitaxy on substrates. The cubic rock-salt structure is the rarest form and can only be found in stable form at extreme pressures (2 GPa).

1.4.2 Toxicology

Generally, zinc oxide is considered non-toxic and is not found, through any authentic studies, to be an irritant, carcinogenic, genotoxic or toxic to human reproductive system. On the other hand, the zinc oxide powder, if inhaled or ingested, can cause a syndrome called zinc fever or zinc ague, characterized by chills, fever, cough and chest tightness. EU hazard classifications categorized the zinc oxide as extremely toxic for the aquatic environment- N; R50-53, although it is essential for humans, animals as well as plants in trace amounts (10-15 mg per day for human metabolism). Thus, the preparation, packaging, transportation and handling of ZnO must be followed through with great care and precautions. The packages must be labelled "UN3077-Class 9, Environmentally Hazardous Substance". Studies have established that the eco toxicity found in the *Tetrahymena thermophila*, an aquatic model protozoan, is caused by solubilized Zn^{2+} ion. The toxicities of zinc oxide ions in bulk, nano and soluble form are quite similar, exhibiting EC_{50} values of around 4-5 mg Zn/L (5 ppm). Various applications of zinc oxide, in nano form, include use in sunscreen products, since 1990s, to neutralize the effects of UV rays. The contemporary studies have confirmed the low levels of systemic toxicity caused by ZnO particles as they do not penetrate the skin cells and hence, can be considered safe for human use.

1.4.3 Morphology of zinc oxide particles

It is interesting to note that zinc oxide (ZnO) possess dynamic morphology which can be tuned by inducing changes through its synthesis techniques, in the pH or the concentration of the reacting molecules and also by changes in precursors. Among different shapes of ZnO, some are nodular (0.1-5m), circular (0.5-10m) manufactured by French and American processes and sponge like ZnO manufactured by wet processes

Nano rods [20,21], Nano plates [23,22], Nanosheets [24], Nanoboxes [22], irregularly-shaped particles (ISPs) [22], polyhedral drums [22], hexagonal prisms, Nano mallets [22], Nanotripods [25], tetrapods [26], Nanowires [27], Nanobelts [27,28], Nano combs and Nano saws [28], Nanosprings and Nanospirals and Nanohelixes [21,105], Nano

rings [21,28], Nanocages [99,28], Nanoneedles [10,29], Nanotubes [10,21,30], Nano donuts [10], Nanopropellers [10], and Nanoflowers [31,30].

1.4.4 Bulk zinc oxide

Mostly the bulk ZnO is produced by American or French processes, their surface area (1 and 10 m 2 g−1) varies depending on the process used. During high manufacturing temperature, crystalline particles are formed. Bulk ZnO having low surface area are not considered active.

Other 'wet-process' ZnO:

Some ZnO are produced using wet chemical processes like precipitation etc., their surface area ranges from 10-30 and 50-60 m2 g−1. Their surface area can be managed by changing the conditions of manufacturing process such as changing the concentration of base method

1.4.5 ZnO single crystals

ZnO single crystals (n or p type) widely used in electronics are manufactured using hydrothermal (350-450 ◦C) growth and 2500 bar pressure conditions or vapor phase transport growth (1100–1400 ◦C) or even at low melting temperatures using pressurized melted salts [8,10,116]. Among all the manufacturing methods, vapor phase method is relatively fast (7-8mm/day). Similarly, low melting temperatures also have a high yield of ZnO at faster rates [112, 38–39]. On contrary, hydrothermal conditions are very slow but have a yield of good large crystals [36, 37].

Compared to n type, p type crystals are manufactured rather hardly but as of recent polycrystalline films are successfully produced

1.4.6 Optical properties

The application of ZnO in optoelectronic applications is reshaping the interest of researchers in ZnO molecules [4, 5, 7, 42]. It is postulated that ZnO based applications are cheaper and non-toxic, thus can be easily used as best alternative for old optoelectronic devices that were based on UV or blue ranges such as LEDs etc. Similarly, ZnO exhibit same band gap energy of 3.37 eV at RT as that of GaN but a far greater exciton binding energy of 60 meV [42]. For improvising ZnO band gap energy,

several options can be utilized such as by alloying with MgO that can increase the band gap of ZnO in the range of 2.3-4.0 eV [49, 39]. In terms of emission properties of ZnO, many factors such as manufacturing methods, size, shape, surface coating ligands etc. largely influence it [49, 50, 41–43].

1.4.7 Electrical, thermal, and magnetic properties

ZnO is in the list of extensively researched semiconductors but difficulties associated with p-type single crystal ZnO manufacturing have caused serious harm to applications of ZnO in a wide range

1.5 Piezoelectricity, pyroelectricity and thermoelectricity

First use of ZnO as a piezoelectric semiconductor having large electromechanical coupling coefficient was discovered in 1960s. Afterwards ZnO was used in surface acoustic wave devices as a thin surface layer, resonators, scanning probe microscopy for controlling tip movement and in air or liquid sensors [50, 28, 42].. This was also mainly due to the tetrahedral coordination in ZnO that incorporates changes in shape of ZnO (non-centro symmetric), thus being piezo and pyro-electric. Moreover, a n-type ZnO i.e. doped ZnO including AI-doped ZnO have applications as thermoelectric compound

It’s Unfortunate that besides all the characteristics of ZnO, it is still limited of use when compare to other thermoelectric substances.

Chapter 2

2 Experimental procedure

2.1 Synthesis of MoS_2

Currently different techniques have been used for synthesizing 2D MoS_2 in bio sensing applications. These methods include sonolysis [51], Plasma microwave [52], Electrochemical/Chemical Method [51, 53], Chemical Vapor Deposition Method [54], Chemical Exfoliation [55] etc. However, on the large scale production, these methods are not appropriate as they produce the low yield and MoS_2 flakes on substrates. In our experiment production of MoS_2 by means of hydrothermal method has been carried out. Hydrothermal method has been used because of following reasons:

- In hydrogen evolution reaction MoS_2 has shown higher catalytic activity when produced through this method.
- The size and morphology of final product can be engineered easily through this method.

2.2 Hydrothermal Method

This method usually involves simple steps. In this method reactants are maintained at low temperature and resultant material also indicated precise size and morphology which in turn enhances the electrochemical properties of material. MoS_2 can be synthesized with more controllable structure by controlling crystallization condition. Through hydrothermal method it become easy to control crystallization parameters. Crystallization of MoS_2 can be controlled by controlling temperature and pressure as both the parameter is in direct relation with crystallinity. In our case we have used different parameter in different experiments for synthesis of MoS_2. We are going to discuss the procedural steps for synthesis of two of them.

The Stepwise synthesis procedure for MoS_2 is given below:

- 0.5 grams of sodium molybdate and 0.175gm of Sulfur are weighted precisely. These reactants are taken out in a stainless steel autoclave of capacity 100 ml.

- Then 0.6 ml of hydrazine is measured with help of pipette. Hydrazine is dropped into previously measured reactants in autoclave.
- Autoclaves are then filled with water and closed tightly.
- Autoclaves are maintained at 150^0C for about 34 hours.
- After 34 hours autoclaves were taken out and allowed to cool at room temperature.
- Resultant material is taken out and centrifuged repeatedly with water and ethanol for about 5 to 6 times.
- After washing material is dried at 60^0C for about 5 hours.
- Finally, material is crushed with mortal and piston and we obtain MoS_2 in form of silvery black colored powder.

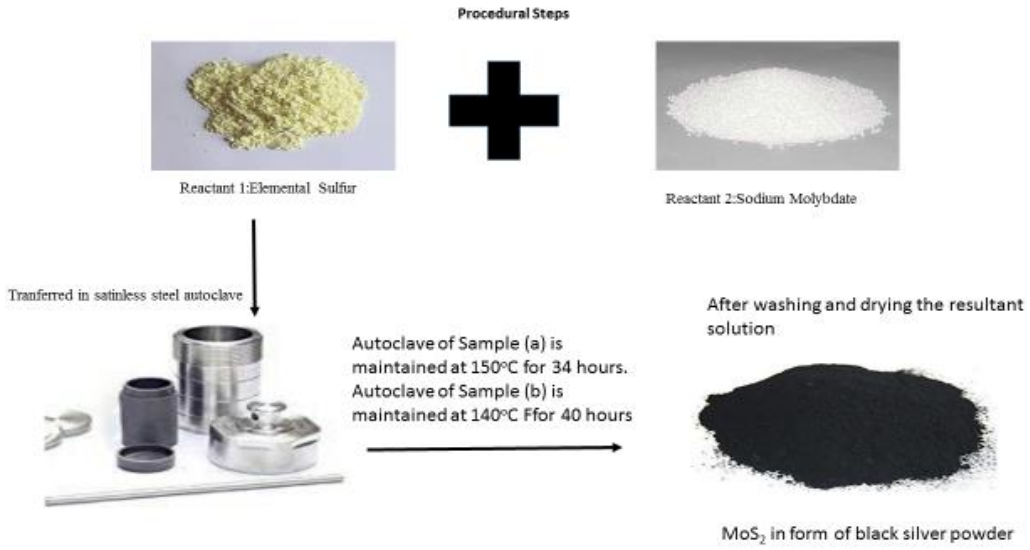

Figure 2-1Synthesis of MoS2

2.3 Synthesis of MoS_2/ZnO

The Stepwise synthesis procedure for **MoS_2/ZnO** is given below:

- 0.5 grams of molybdenum di sulfide is weighted.
- 0.378 grams of zinc nitrate hexa-hydrate is added to the solution.
- Autoclaves are then filled with solution and closed tightly.
- Autoclaves are maintained at 80^0C for about 6 hours.

- After 6 hours autoclaves were taken out and allowed to cool at room temperature.
- Resultant material is taken out and centrifuged repeatedly with water and ethanol for about 5 to 6 times.
- After washing material is dried at 60^0C for about 5 hours.

2.4 Biosensor

A biological sensor is an analytical device which contain immobilized biological component e.g. enzyme, antibody or nucleic acid etc. These biological components interact with analyte to produce physical, chemical or electrical change which is measurable. An analyte is usually a compound like glucose, urea or drug etc. [56]. Bio-sensor involves the conversion of biological actions in measurable signals for quantitative analysis. Bio-sensor has two components

Biological components i.e. Enzyme or cell etc.

Physical component i.e. amplifier etc. [57].Fig 2.2.1 depicts the elements of biosensors.

Biosensor consist in of

- bio receptor binding to analyte
- interface where specific biological event takes place
- Transducer signal which get convert into electronic signal and amplified by detector circuit.
- a computer software to convert signals into meaningful parameters
- a human operator

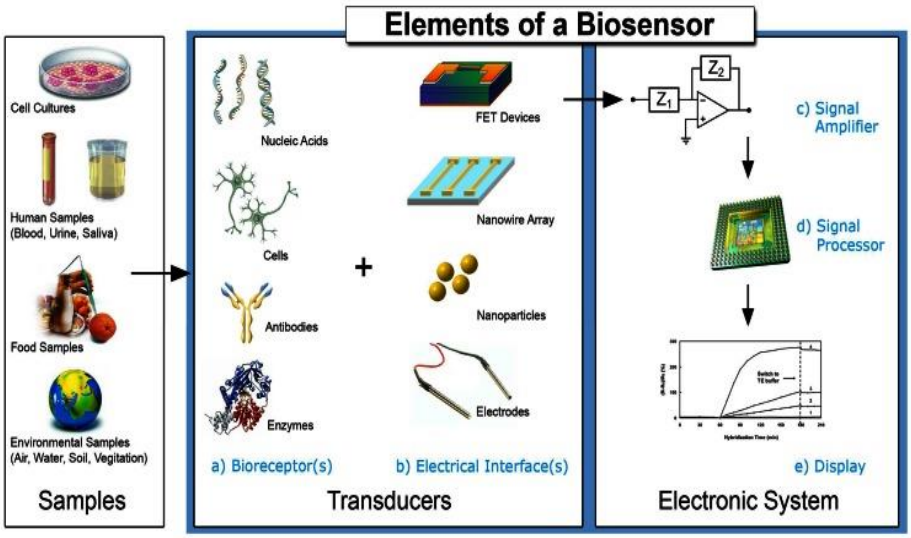

Figure 2-2Elements of Biosensor

2.4.1 Principle of Biosensor

The desired biological material is made immobilized by physical or membrane entrapment, covalent or non-covalent bonding. A bound analyte can be prepared by binding analyte to biological material, which in turn produce measureable electronic signals (56,58).

Principle of Biosensor:

Electrochemical biosensors are devices which work on principle of measurement of electronic current, ionic or conductance charge carried out by electrodes. Electrochemical biosensor contains three electrodes, a reference electrode, a working electrode and a counter electrode. Reference electrode is used to maintain a stable potential by placing it at a distance (58). The job of transduction element in biochemical reaction is performed by working electrode [59]. While connection to electrolytic solution for production of current is provided by counter electrode, Platinum, gold, carbon and silicon electrode are mostly used because of their stability and conductivity. Information about analyte can be obtained by changing potential and then measuring the resultant potential. For this purpose Cyclic voltammetry is a widely used technique which measure the redox potential and electrochemical reaction rate [57, 58]. The voltage is calculated between reference electrode and working electrode while current is calculated between counter electrodes and working electrode. The obtained parameters

are plotted as current vs. voltage also known as voltammogram. Enzymes are also used in electrochemical sensing. Most commonly used one is GOx. Glucose oxidase catalysis the oxygen and glucose reaction in which gluconic acid and hydrogen peroxide are formed which is detected on modified electrode. The reaction of this enzyme is given as follows

O_2 + Glucose → H_2O_2 + Gluconic Acid

H_2O_2 + Donor → H_2O + Oxidized Donor

2.5 Fabrication of Amperiometric Glucose Biosensor

To fabricate the biosensor, prepared material is transferred to a 3mm diameter conventional glassy carbon electrode. A thin film of 5µL nafion solution is dropped onto electrode which attaches the MoS_2 tightly on the surface of glassy carbons electrodes. after the water evaporates, 5µL GOx solution placed on the surface of film. The immobilized GOx was removed through extensive washing and modified electrode was kept in refrigerator at 4^oC overnight

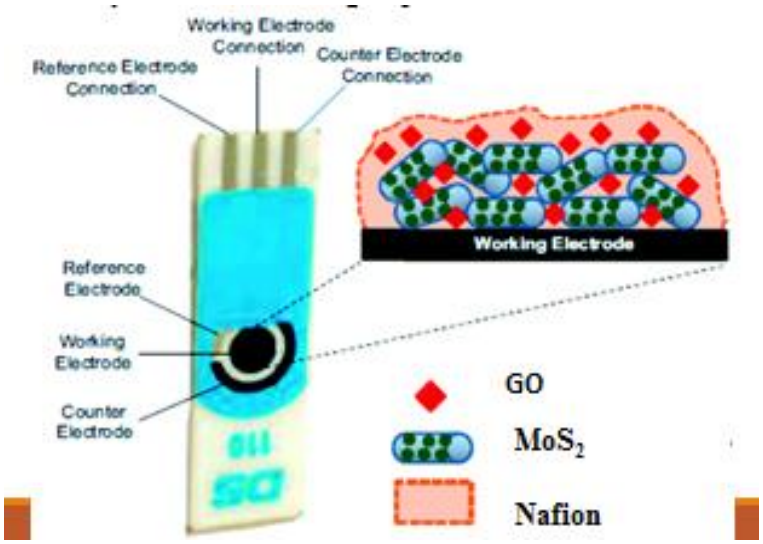

Figure 2-3Fabrication of Electrode

The basic assumption for meaningful XRD is homogenous, angular and spatial distribution of sample in all the directions before exposing the sample to x-rays source [61].

2.6 Photo-catalysis

Photo catalysis is the chemical reaction which occurs when the photons absorbed by solid material which behaved as photo catalyst (Ohtani, 2011). However, the definition of photo catalytic process is still not clear (Mills and Le Hunte, 1997). It is important to note that photo catalyst remains unchanged chemically during and after the photo catalyst reaction. In the literature, the term "photo catalyst" is often used equivalent with term "catalyst". photocatalytic materials behaves differentially in catalysis reaction and thermodynamic reaction. It is because photocatalytic materials behaves as catalyst during the catalysis reaction. Therefore, photo catalysis (DG>0) occurs in the energy storing reactions while catalysis is restricted to thermodynamically possible reactions (DG) (Ohtani, 2010). The photo catalytic activity determine the reaction rate (absolute or relative) of the photocatalysis (Ohtani, 2011).

Five steps are well-known during photocatalysis (Herrmann, 1999):

- shifting of pollutants to the photocatalyst's surface
- pollutants absorption on the surface
- photonic activation and decomposition of adsorbed molecules
- reaction product's desorption
- removal of reaction products from the photocatalyst's surface

Photocatalysis principal explained by the universally accepted theory very well. It is explained in the theory that when a light energy band gap is equal to or larger than the photocatalytic material strike with the photocatalyst, it generates the electron hole pairs which split into electrons (e) in conduction band and holes (hþ) in valance band. The oxidation reduction reaction takes place on the surface of the photocatalytic material following the generation of e and h þ. Often it is happened that the electron-hole recombine which can reduce the chance of the oxidation reduction reactions on the photocatalytic material. Electron-hole recombination determines the reaction rate while the current findings in the field disprove the electron hole recombination during photocatalytic process (Ohtani, 2013).

Another phenomena is explained which happens due to the presence of photocatalyst, UV-vis radiation and ozone is the photocalytic ozonation. In this reaction, when the photoexcitation of the electrons takes place on the surface of the photocatalyst, ozone molecules adsorbed on the surface of photocatalyst which leads to the formation of active oxygen radicals which when reacted with water molecules, form the hydroxyl radicals (Huang and Li, 2011). Moreover, it is also reported that when ozone absorbs a wavelength shorter than 300 nm (Mehrjouei et al., 2015) active oxidizing species are produced O3 þ hv / O þ O2.

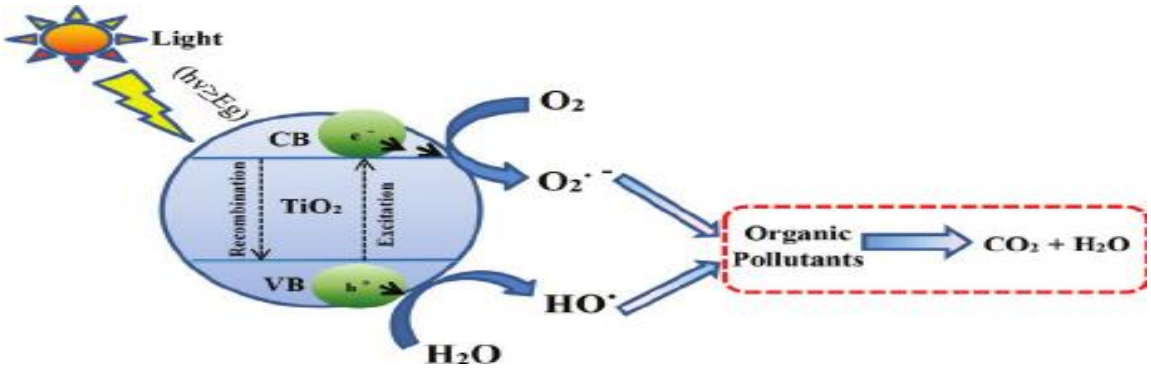

Figure 2-4Schematic of photocatalysis

2.7 Literature review

Amperometric glucose biosensor are highly sensitive in which single ZnO Nano fiber (ZONF) is used Ahmad et al (2010). Nano fibers (NFs) of poly (vinyl pyrrolidone)/zinc acetate composite are used to synthesize by electro spinning technique. ZONFs have been successfully obtained in the range of 350-195 nm diameter by elevate the temperature in order to calcinate the above precursor fibers. Concerning its function, through the physical adsorption single NF on a gold electrode worked with glucose oxidase (GOx). Biosensor detect the high and reproducible sensitivity of 70.2 μA cm-2 mM-1 within a response time of less than 4 s which also showed a linear range from 0.25 to 19 mM with a low limit of detection (LOD) of 1 μM. These biosensors also possess the influential anti-interference ability and promising stability for long-term storage (more than 4 months). All of these characteristics highly support that a biosensor

can be designed through individual ZONF and can be used for other biological applications.

Xiong et al (2018) reported that the MoS_2 layer-structured only suitable for hydrogen evolution reaction (HER) and not for oxygen evolution reaction (OER). In order to obtain the bi-functionality of HER and OER onto MoS_2 , a cobalt covalent doping approach was used which surprisingly boost the HER activity as well as OER activity. The conditions used to achieve this activity are the HER and OER onset potentials of −0.02 and 1.45 V (vs reversible hydrogen electrode (RHE)) in 1.0 m KOH. In particular, low HER and OER over potentials of 48, 132, 165 mV and 260, 350, 390 mV can pass on the high current densities of 10,100, and 200 mA cm−2. Other transition metals can be used to achieve the bi-functionalization by using catalyst activation approach.

Ahmad et al (2009) investigated the synthesis of amperometric biosensor which is highly sensitive. These biosensors have been made by incorporated the Pt onto ZnO which formed a hybrid nano spheres. These Pt-ZnO Nano spheres (PtZONS) ranged 50-200 nm diameters by depositing the electrons on a glassy carbon electrode (GCE). High resolution transmission electron microscopy (HRTEM) and energy dispersive X-ray spectroscopy (EDS) have been used to identify the Pt Nanoparticles in ZnO Nano spheres. The doped Pt Nanoparticles has the ability to oxidize the hydrogen peroxide through electro catalysis which considerably elevates the response current. The PtZONS/GCE shows the high sensitivity to hydrogen peroxide is 147.8 μA μM-1 cm-2. Cholesterol oxidase (ChOx) is used to functionalized the PtZONS/GCE through physical adsorption. The enzyme electrode is highly sensitive to cholesterol as it detects the sensitivity of 1886.4 mA M-1 cm-2 in less than 5 s of response time and shows the linear range from 0.5 to 15 μM. Furthermore, biosensors good anti-interference ability and favorable stability suggest them to use over the longer period of time. All of these characteristics suggest the PtZONS highly sensitive to cholesterol but also use the low potential to drop the interference.

Wang et al (2014) developed a series of MoS_2 Nanostructures by using the one-step hydrothermal process in which he changed the surfactant as soft template and

temperature of hydrothermal reaction. He used the different techniques to investigate the three type of MoS_2 Nanostructures three-dimensional (3D) which are hierarchical Nano spheres, one-dimensional (1D) Nano ribbons and large aggregated Nanoparticles. Different techniques which he used were X-ray diffraction (XRD), field emission scanning electron microscopy (FESEM), high resolution transmission electron microscopy (HRTEM), and Brunauer–Emmett–Teller analysis (BET). MoS_2 Nanostructures involves the multiple cycles and are capable to carry the high initial discharge potential (higher than 1050.0 mA h g1). The structure of the MoS_2 Nano spheres revealed the sheet-like subunits with the highest particular potential of 1355.1 mA h g1, and 66.8% with the maintenance even after 50 cycles. The hierarchical MoS_2 Nano spheres have the good lithium storage characteristics which can help in large electrolyte/ MoS_2 contact area and stable 3D layered structure.

Molybdenum disulphide particles and complex composites have been investigated for a long period of time for the synthesis and application of Nanostructure Bazaka et al (2019). Molybdenum has the transition properties while sulfur has the high chemical activity. To achieve the molybdenum disulphide Nanoparticles, nucleation, growth, and shaping is involved in the process. Apart from the understanding of biological and catalytic activity, some questions remain unclear and need to be addressed. Recent progress regarding the nucleation and growth of various molybdenum disulphide give rise the idea to use the Nanostructures for the visualization of important fabrication methods spectrum which can be from the simplest solution-based techniques to the most advanced chemical vapour deposition and plasma-enhanced chemical vapour deposition techniques. Nanostructures have been widely used in medicine, for the anti-cancer therapy, drug delivery and medical imaging. At present, its most challenging to maintain the balance between the particle structure and chemical activity during synthesis, since molybdenum disulphide Nano-structures have been used in advanced biomedical applications.

Li et al (2014) investigated the different kind of MoS_2 Nanostructures which can be synthesized by using the sulfur containing reagents such as carbon disulphide CS2, Anhydrous Sodium sulphide Na2S, Thioacetamide CH3CSNH2, Ammonium thiocyanate CSN2H4, and Potassium thiocyanate KSCN. Designed solution chemical

reactions of Na2MoO4 also used for the synthesis of nanostructures e.g hollow-cage fullerene-like particles, fibrous floccus, and spherical Nano vesicles. Experimental data shows the possible redox reaction routes which revealed the Mg2+ ions in synthesized MoS_2 nanostructures possesses the preferable reversibly intercalation/deintercalation cycles than in bulk MoS_2 samples. Different techniques have been used to characterized solution product of MoS_2 and their samples which required high temperature for annealing by X-ray powder diffraction (XRD), transmission electron microscopy (TEM), X-ray photoelectron spectroscopy (XPS), and resonance Raman spectra.

Luxa et al (2016) also investigated the MoS_2 and WS2 synthesis through thermal reduction of tetrathiotungstate/tetrathiomolybdateand graphite oxide on a conductive graphene support. During the synthesis , a byproduct Magnli is formed which greatly influenced the catalytic properties towards hydrogen evolution whereas the catalytic activity towards oxygen reduction of these composite materials is not affected by this phenomenon. For the industrial purpose this phenomena is of great importance because of the high catalytic activity Hussain et al (2016) used the co-precipitation method to evaluate that Flower shaped hierarchical Zinc oxide Nanostructures have been hydrothermally functionalized with 8 nm Au NPs and 15 nm Ag Nanoparticles and also investigated the photocatalytic and electrochemical activity of these structures. Moreover several studies conducted to demonstrate the strong interaction between noble metal Nanoparticles (NPs) and Zinc oxide Nano flowers. XPS research theory confirms this interaction. The near band edge transition causes UV emission in PL spectra results in reduced PL intensities of Au–ZnO and Ag–ZnO composites which enhance the photocatalytic activity that happens as a result of increase defects. Moreover, Au NPs shows the higher catalytic activity and stability. ZnO surface also contain the Au NPs which is reported as the source of enhance photocatalytic activity when compared to Ag–ZnO and pure ZnO. Ag–ZnO-modified glassy carbon electrode also known for good amperometric response to hydrogen peroxide (H2O2), with linear range from 1 to 20 lM and detection limit of 2.5 lM (S/N = 3). And also its sensor shows the high detectability y as compared to pure ZnO and Au–ZnO-based sensors. Above mentioned results revealed the different ways to use the efficient non-enzymatic biosensor and environmental friendly remediators.

Li et al (2013) used the novel dual-petals Nanostructured WS2@ MoS_2 heterojunction to explore the photo catalyst which help in the photo degradation of methylene blue. Synthesis process of Nano petals (NPs) structured WS2 includes the pretreatment of ball milling which behave as the base on which the MoS_2 sub-NPs develop. dual-petals Nanostructured WS2@ MoS_2 display the unique structural features which present the numerous active sites which ultimately increase the photocatalytic activity and surpass the pristine MoS_2/WS2. WS2@ MoS_2 composite is extensively studied its structural, electronical, and optical properties which revealed the difference in band gap of WS2@ MoS_2 composite and pristine WS2 and MoS_2. It is appeared that WS2@ MoS_2 composite band gap was narrower with well-defined stagger type-II band alignment resulted in the introduction of the photo excited electron into conduction band minimum (CBM) of MoS_2 from the CBM of WS2. This will block the combining of the photo generated pairs and extend the carriers lifetime and help in proper interface charge distribution. These results will help to understand the composite improved photocatalysis and will open the many applications for the future use.

Jhang et al (2017) developed the ultrathin two dimensional (2D) MoS_2/WS2 Nanosheets having the hierarchical structure by using the facile one-pot hydrothermal reaction. Several methods were applied to inspect the thickness of ultrathin Nano flakes. Three techniques were used named Scanning electron microscope (SEM), transmission electron microscope (TEM) and photoluminescence (PL) which revealed the nanoflakes thickness of 2–10 nm. Nanoflakes heterostructure helps to separate the electro–hole pairs. Vertical structure of Nanoflakes increase the surface area as it exhibits the unsymmetrical structure. MoS_2/WS2 hybrid present improved photo and electrochemical behavior than the pure MoS_2 or WS2. In electro catalytic hydrogen evolution reaction , it can be used as photocathode.

Zafar et al (2016) worked on the Optical emission efficiency which is the most significant characteristic of the two-dimensional layered transition metal dichalcogenides (TMDs) and can change the optoelectronic performance. In order to achieve the optoelectronic-grade quality , it's necessary to optimize the growth parameters through the chemical vapor deposition (CVD). This study uses the systematic photoluminescence (PL) spectroscopic approach to evaluate the intrinsic optical and crystalline quality of

CVD grown MoS_2 (CVD MoS2). For this purpose, intensity ratio is measured in air and vacuum. By growing the MoS_2 at different temperatures helps to detect the structural defects. For often low temperature measurements helps in the detection of structural defects. This will help in the development of optoelectronic devices through the alteration in growth parameters.

Naaz et al (2019) used the one pot synthesis technique to investigate the Silver Nanoparticles embedded in graphene oxide (Ag-GO) Nano composite which is further analyzed by using the different techniques e.g. FESEM, TEM, EDX, XPS and Raman spectroscopy. The Nano composite shows the several advantageous activities including the upgraded photo catalytic and antibacterial activities but also better biocompatibility. It is also resistant to bacterial growth. The composite also shows the nontoxic behavior. Moreover, Ag-GO Nano composite also degraded the toxic organic dyes rapidly which is five times higher than the alone GO. Enhanced biocompatibility, photo catalytic degradation activity made it good for the commercial use

Chapter 3

3 Characterization techniques

3.1 Characterizations

Characterization techniques are used to explore the different aspects of Nanomaterials including its morphology, surface properties, composition, purity and stability and also study their advantages and disadvantages [62]. These techniques are basically divided into two major categories: The techniques which are used to study the structural and elemental composition and those which are used to explore different optical and electrochemical properties. According to the regulatory guidelines, these techniques for characterization of Nanomaterials are fundamental to ensure the safety of Nanomaterials [59]. The characterizations which are used for various analyses of Nanomaterials are given below

- **Characterization of Structural and Elemental composition analysis:**
  - Energy Dispersive X-ray Spectroscopy (EDX)
  - X-ray Diffraction (XRD)
- **Characterization of Optical Properties analysis:**
  - Fourier Transform Infrared Spectroscopy
  - Raman Spectroscopy
  - UV-VIS Spectroscopy
- **Characterization for Studying Morphology:**
  - Scanning Electron Microscopy (SEM)

The above-mentioned characterizations are discussed below separately.

3.2 X-Ray Diffraction

X-Ray Diffraction technique was used to examine the structural properties of material which tell us about the phase identification of materials. It works on the principal which

describes the X-Rays compatible range in crystal which is distance between atoms. When the X-Ray hits the crystal, x-rays diffracted and display the different lengths with different sharp points. The interaction between x-rays and crystalline material is explained with Braggs Law [59].

According to brags law, when the series of planes of crystal fall on X-rays, it reflects. After reflection, when the angle of incident is equal to angle of reflection during that period reinforcement of waves reaches at its highest points. Waves from successive layers reinforce when their path differences integral multiple of "λ". If we examine the crystallographic structure maintained the distance between the planes equal to "d" and X-rays of wavelength "λ" to be incident upon them, then according to Bragg's Law:

$\lambda=2d\sin\Theta$…….3.1.1

Where "Θ" represented the angle between crystal planes incident beam. For constructive interference the equation becomes:

$n\lambda=2d_{hkl}\sin\Theta$…….3.1.2

Where h, k, l are miller indices. Constructive interference shows sharp peaks which will determine phase of crystals. [63].

3.2.1 Sample Preparation for XRD Analysis

As the quality of the collected data is totally dependent upon the sample quality and to the standard of its preparation and deposition [60]. The success of structural analysis is associated with type of sample and on experimental conditions. A fine grinded powder serves as a sample for structural analysis. A common mortar and pistel can be used for this purpose as shown in the figure 2.4(a) below. Bulk MoS_2, ZnO and MoS_2/ZnO was grinded with help of mortar and pistel. Then grounded powder was deposited on sample holder which could be of aluminum, plastic or glass as shown.

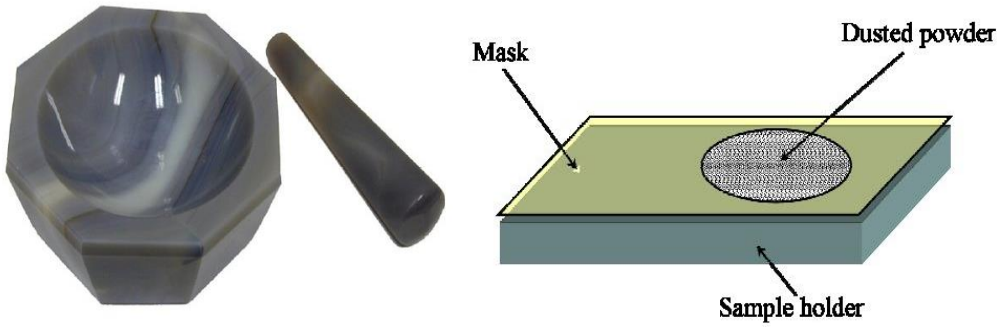

Figure 3-1Agate mortar pestle, XRD sample preparation

3.3 Scanning Electron Microscopy

Electron microscopes are scientific instruments in which samples are investigated at very fine scales. SEM is used to visualize the surface of the object and provide information about morphology of the material [64]. In SEM electrons are produced by tungsten wire when it is heated by current. High electrical field gradient is provided to accelerate the electrons. Inside high vacuum column, electronic lenses are used which helped these "primary electrons" to concentrated and diverted to give rise to a narrow scan beam which then bombard on target. Electrostatic and magnetic fields are applied to control the direction of travelling of electron beam. Area of object can be covered by scanning simultaneously in two perpendicular directions. Secondary electrons are produced from each mark of specimen. The angle and velocity of these electrons are in connection with surface structure of object. Detector collect he secondary electrons to form the image of specimen [65].Parts and arrangements of SEM can be observed from Figure 12.

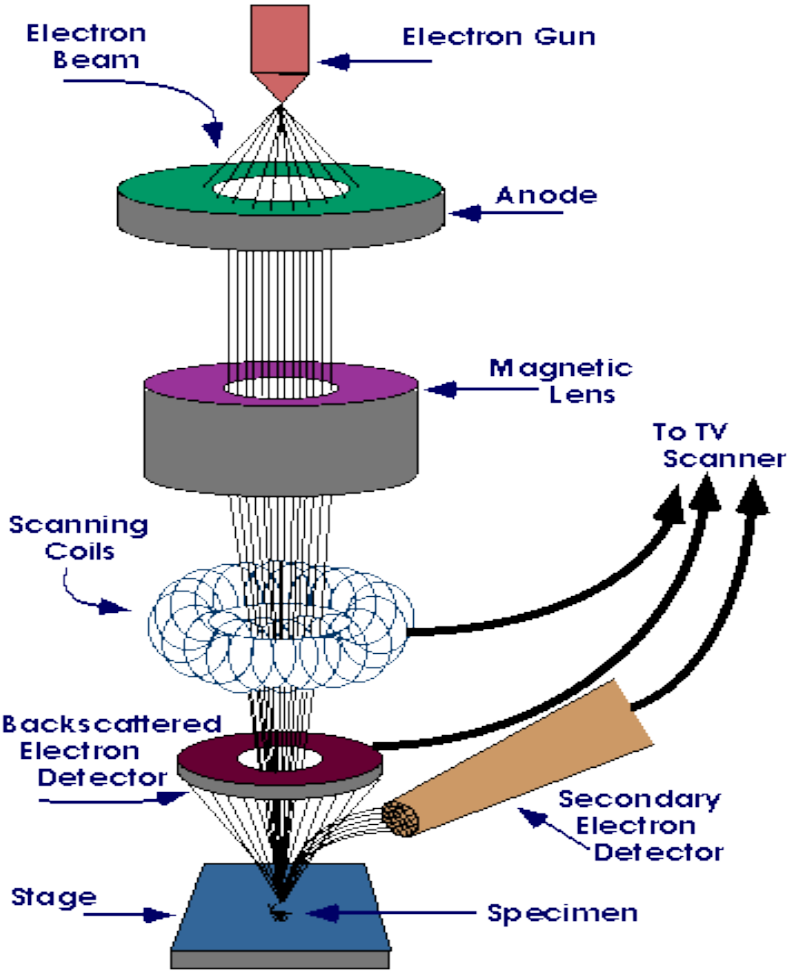

Figure 3-2 SEM Elaboration

Parts of SEM and Their Working:

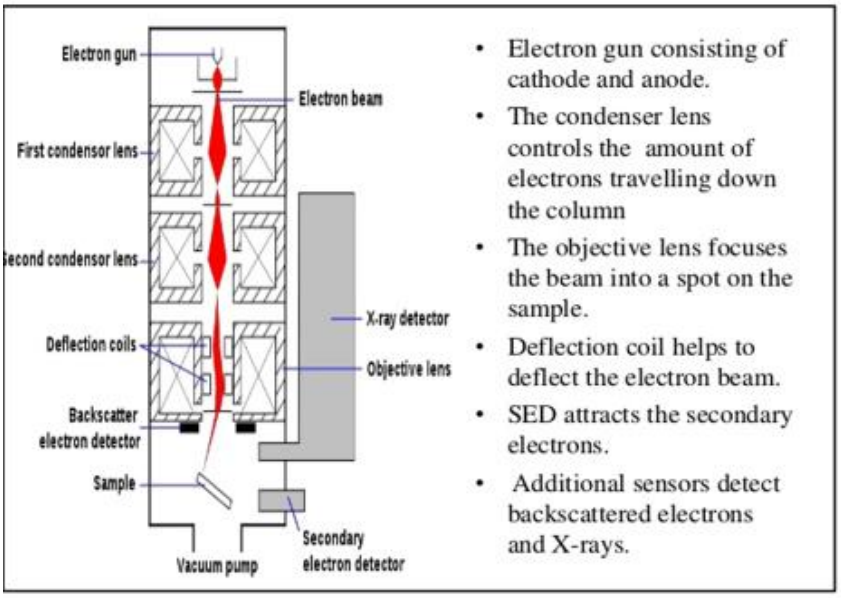

Figure 3-3 Working of SEM

Although SEM is a large expensive piece of equipment still hey remain popular among researchers due to high resolution and detail image, produced by them [66].

3.3.1 Sample Preparation for SEM

Sample preparation plays a vital role when dealing with obtaining information's from scanning electron microscopy. To obtain the proper information sample should be made conductive. Metals need no preparations to be conductive as they are already conductor but nonconductors need to be coated with conducting materials. This job is usually performed by sputter coater. First sample is cleaned with ethanol and placed in ultra-sonic bath for about 20 to 25 minutes. Than small amount of sample was deposited on already cleaned silicon wafers with help of pipette and dried. Before maintaining sample in vacuum environment complete dryness is very necessary as water molecules can produce obscurity in images after interacting with electron beam. Then in order to make MoS_2 conductive for electron beams, sputter coater was used which is shown in Figure 10 Process of sputtering was continued for about 15 sec to deposit a layer of gold on samples. After maintain sample in clean environment for 24 hours, samples are mounted

on sample stubs, using conductive double coated carbon tape as an adhesive for this purpose. Stubs and tapes can be viewed in Figure 11.

Figure 3-4 Scanning Electron Microscope

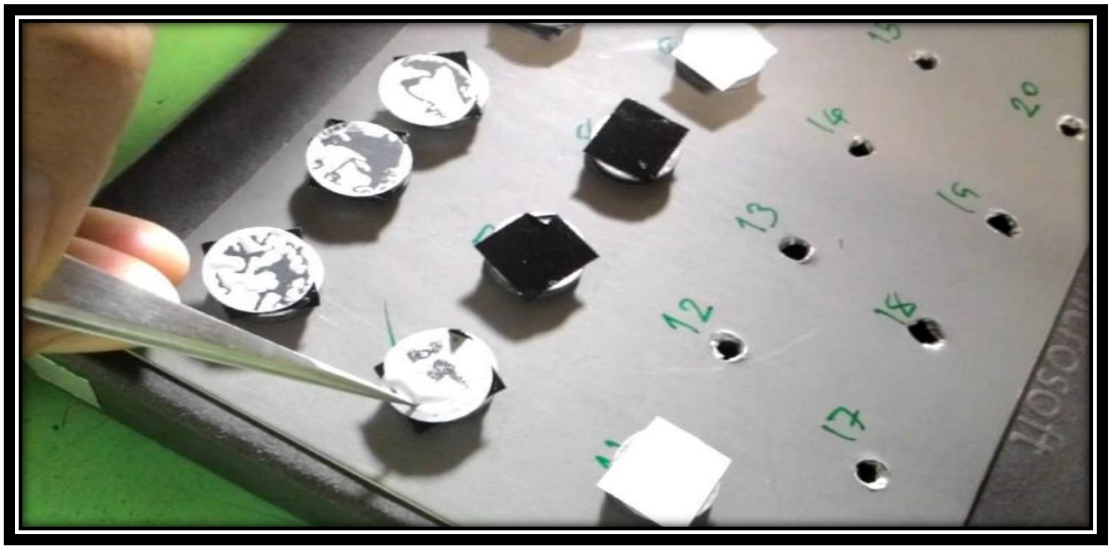

Figure 3-5 Stubs for SEM Sample

3.4 Fourier Transform Infrared Spectroscopy

FTIR spectrometers (Fourier Transform Infrared Spectrometer) has numerous applications and are broadly used in

- Organic composite,
- Macromolecular science,
- Petrochemical engineering,
- Pharmaceutical industry
- Food analysis.

In the 19th century, infrared lights were discovered which gave the scientists a new platform to utilize the infrared light in multiple ways for different purposes [67]. Infrared spectrum contains the vibrating molecules which when show to infrared radiation, they absorb the radiation of particular wavelengths, results in the change of dipole moment of molecules. Their energy level changes from ground state to excited state [68]. Vibrational energy gap tells the frequency of the absorption peak. Vibrational freedom of the molecule will generate the number of absorption peaks which will tell the change in dipole moment and possible energy levels transition. Infrared spectrum can be used to gain the information about the structure [69]. The unique aspect of infrared absorption is its capability to analyze the samples in all three states. Most common used region of infrared absorption spectroscopy lies 4000 ~ 400 cm^{-1} because the organic compounds and inorganic ions absorption region falls in this range [70].

3.4.1 Working of FTIR

A common FTIR spectrometer has the following components

- a source
- interferometer
- sample compartment
- detector
- amplifier
- A/D convertor and
- a computer [71]

The source produces the radiation which transfers the sample through the interferometer and fall onto detector. After the detector, detect the sample it generates the signal which is then amplified by the amplifier and converted to digital signal through analog-to-

digital converter, respectively. Afterward, the signal is transferred to a computer in which Fourier transform is carried out. Figure 13 is a block diagram of an FTIR spectrometer which also reflects the working of FTIR Spectrometer.

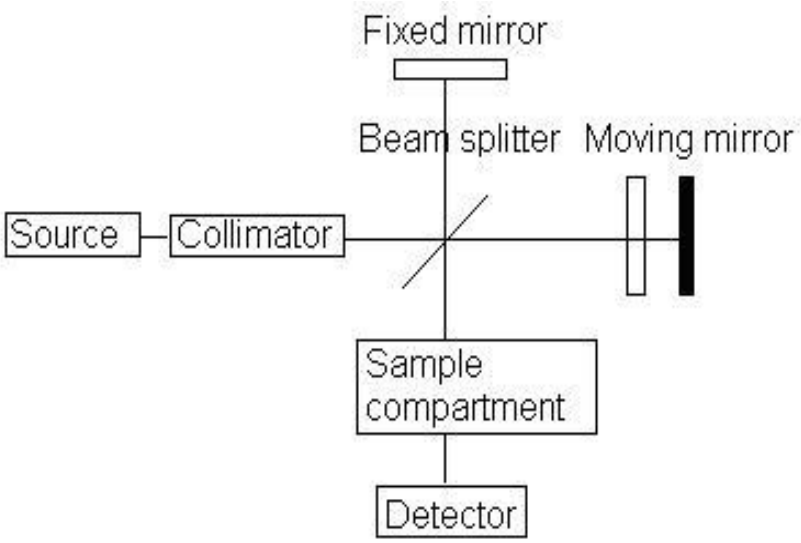

Figure 3-6 Working of FTIR

3.5 Raman Spectrometry

C. V Raman is the Indian physicist who developed the Raman spectroscopy which is used to detect the different types of movements in a system e.g vibrational, rotational, and other with low frequency [72]. Monochromatic light in the visible either close to infrared, or ultraviolet range generates the inelastic dispersion, or Raman scattering. The collision of laser light with the molecules, changes the photons energy level [73]. The change in energy level will tell about the vibrational modes in the system.

When the light hits the molecule, it disturbs the electron cloud releases the photon and excites the molecule from its ground state to high energy level. When it relaxes, it releases the photon and returns to a different state. This process is called Raman effect [74][75]. The difference in energy will determine the emitted photon frequency. If the final vibrational state of the molecule has the higher energy than the initial state, than the emitted photon will be move to lower frequency, which keeps the total energy of the

system in balanced state. This phenomena of shift in frequency is called stokes shift. If the final state has the lower energy than the initial state, emitted photon will be moved to higher frequency. This phenomenon is called anti-stoke shift [76].

3.5.1 Working of Raman Spectrometer

Conventionally, laser beam is used to illuminate the sample which is collected with a lens and sent through a monochromatic. Due to the elastic Rayleigh scattering some wavelengths lie close to the laser line are filtered out while the rest of the collected light is dispersed onto a detector [77]. The main disadvantage of the Spontaneous Raman scattering is its weak scattered light, which is difficult to separate the weak in-elastically scattered light from the intense Rayleigh scattered laser light [78]. Following figure 14 represents the working of Raman spectrometer graphically.

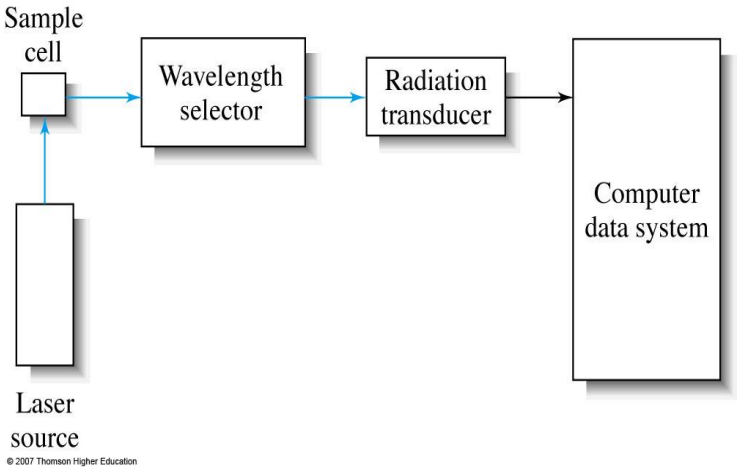

Schematic of Raman Spectrometer

3.6 Transmission Electron Microscopy (TEM)

In material science, transmission electron microscope is the necessary tool as it is used to study the structure of semiconductors. The working principal of TEM used the high energy beam of electrons which are then focused on very thin samples. The interactions between the electrons and the atoms act as a source to observe features [79].

Parts of TEM

Parts of TEM re shown in Figure 15.

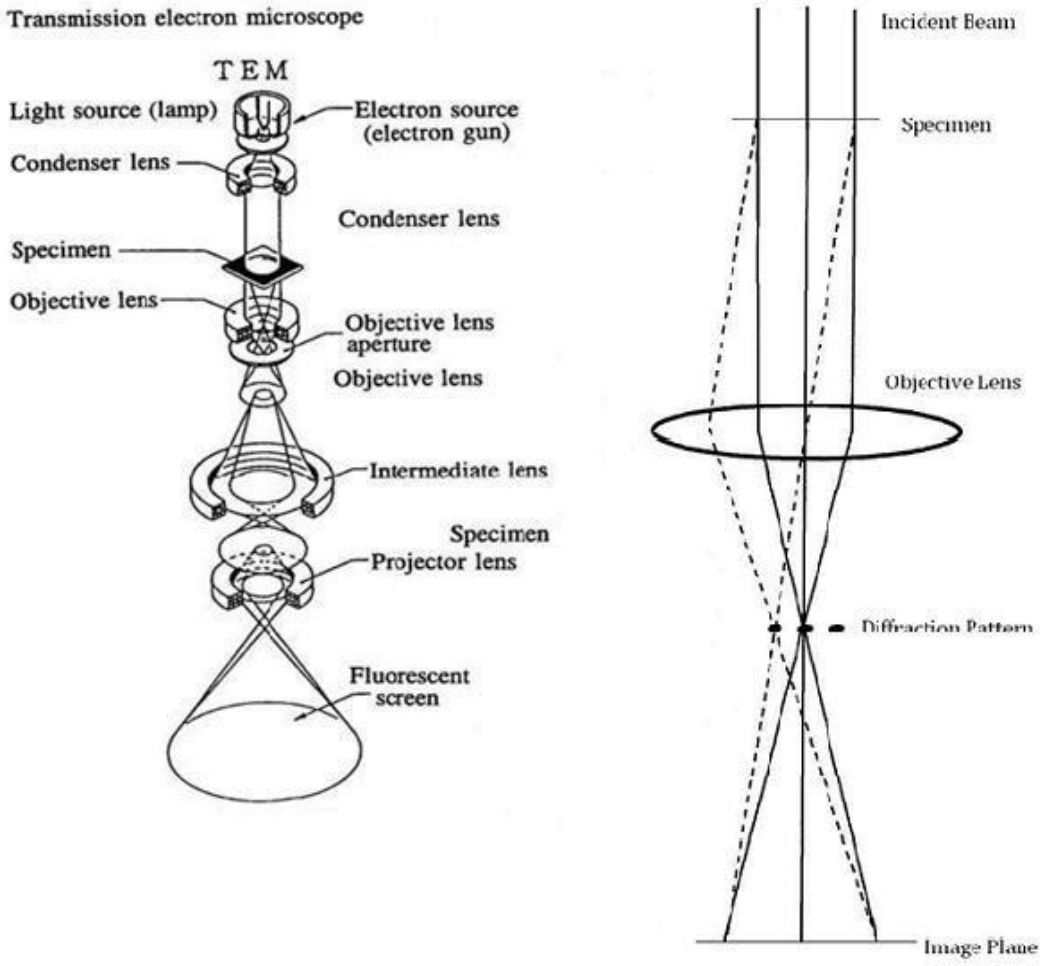

Figure 3-7 Parts of TEM

3.6.1 Working of TEM

The TEM uses the electron for its operation which gives the high optimal resolution for TEM images because of the smaller wavelength of electrons and help to see the finest details of the internal structure [80].

3.7 Cyclic Voltammetry

Electric cyclic voltammetry is a type of potentio-dynamic which measures the electrochemical reaction. For the most time, voltammetry is used to study the redox properties of the materials. In the experiment, solution contains the electro active species and the three electrodes while the electro potential remains same during the experiment. The potential of the working electrode rise linearly as the time passes. Electrolyte is added in the solution to check the conductivity. All of these components collectively will determine the range of potential. In CV experiment, potential and current is measured between the three electrodes. Potential is regulated between reference electrode and working electrode while current is regulated among counter electrode and working electrode. When the potential equals to reduction potential of analyte, current will elevate. After that, potential of working electrode will increase in opposite direction and generate the current of reverse polarity.

The measurement is taking between current and working electrode verses applied voltage of working electrode to give cyclic voltamogram trace.

The electro chemical measurements are taken at room temperature by exercising the electro chemical workstation and configure the three electrodes. The glassy carbon electrode was used as working electrode and platinum as counter electrode. The PH meter was used to measure the pH of solution in real time.

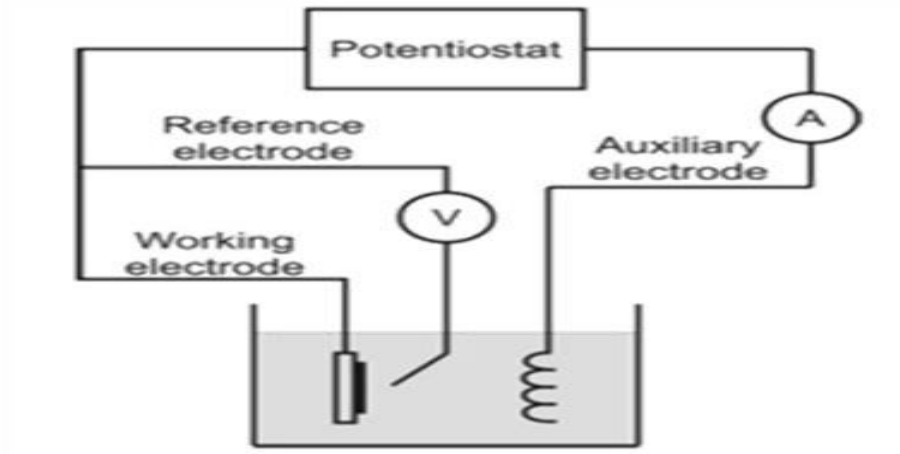

Figure 3-8 Cyclic Voltammetry Setup

Chapter 4

4 Results and discussion

4.1 SEM

Scanning electron microscopy (SEM) images along with the energy-dispersive X-ray (EDS) for elemental analysis were obtained on FEI Nova NanoSEM 450. MoS_2 Nanoparticles have been exhibited by Fig 1. It illustrates that MoS_2 Nanoparticles have rod like nature as it has been shown in the pictures. EDX analysis has also shown that Mo and Sulphide contents have been present in this sample. While in Figure 2. ZnO Nanoparticles have been shown which exhibit arrays structures at different resolutions and along with it EDX results have also been matched. Lastly in Fig 3. the composite of ZnO/ MoS_2 has been visualized at different resolutions. It has been observed that ZnO particles have been successfully coated onto the MoS_2 surfaces and later EDX studies also reveal the complete synthesis of ZnO/ MoS_2 composites.

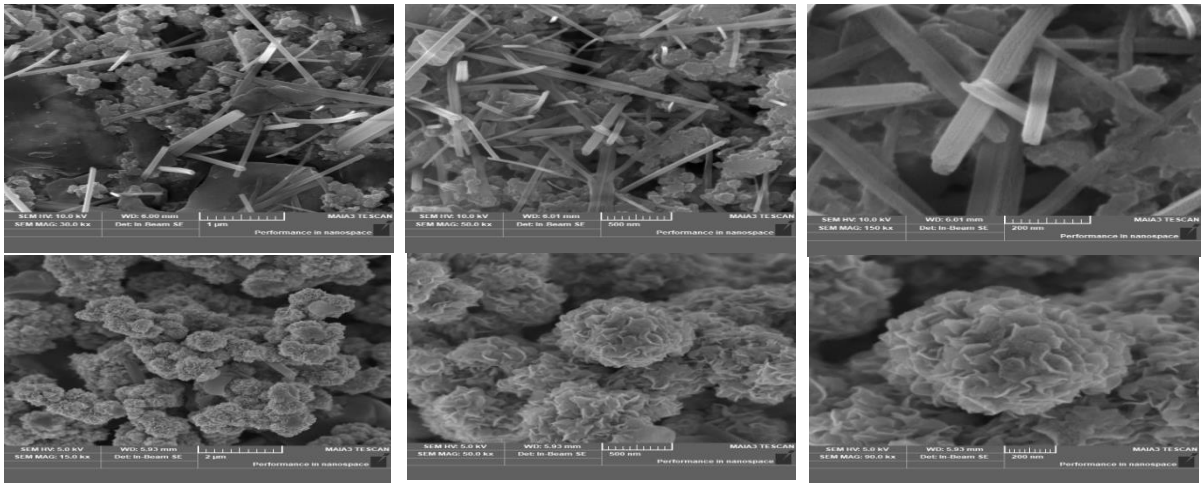

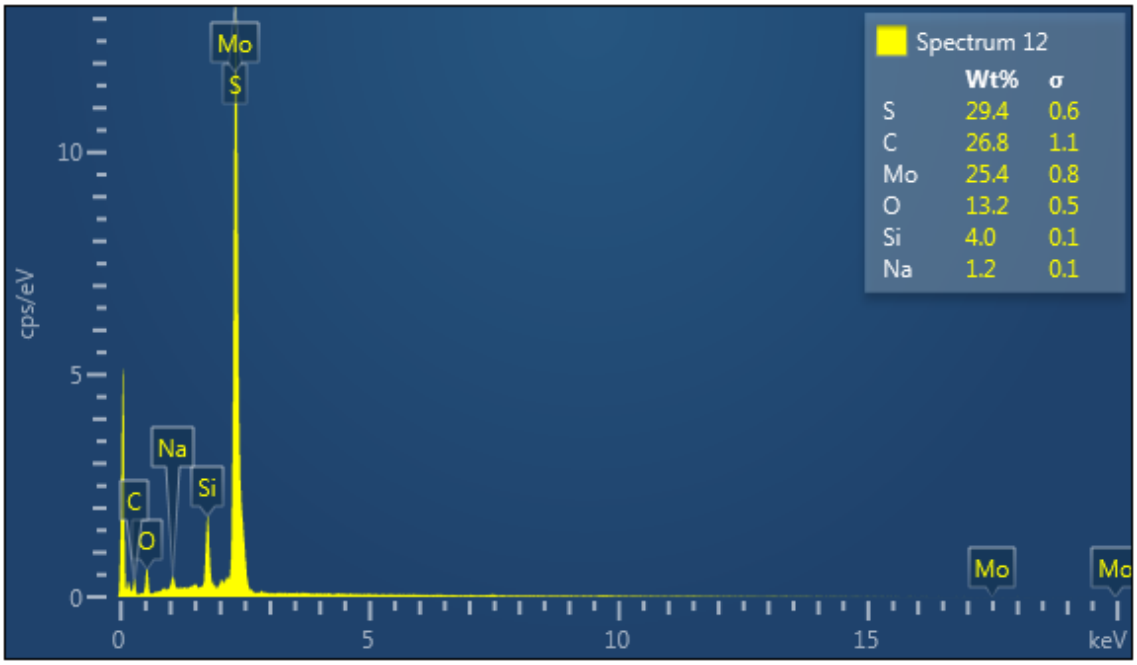

Figure 4-1 SEM images and EDX analysis of MoS_2 particles

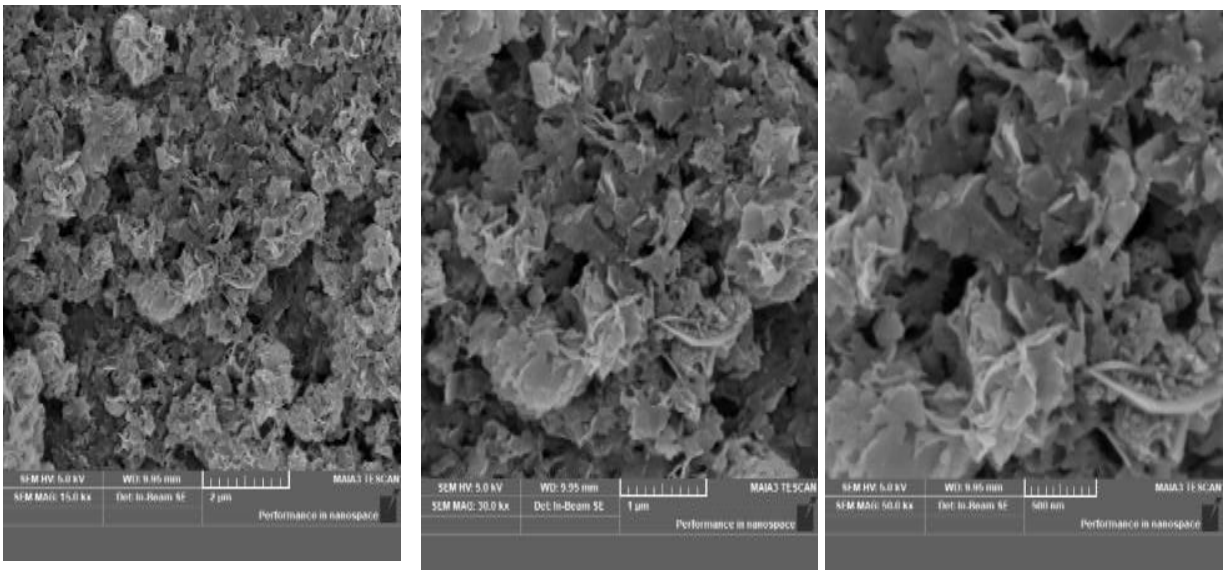

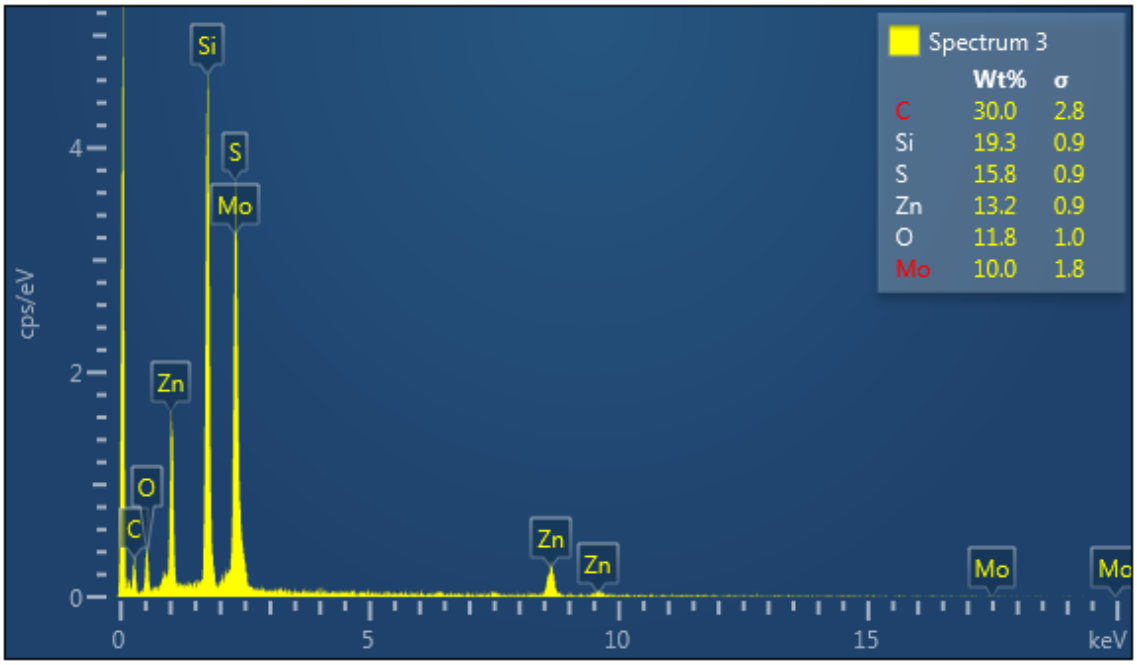

Figure 4-2 SEM images and EDX analysis of MoS_2ZnO

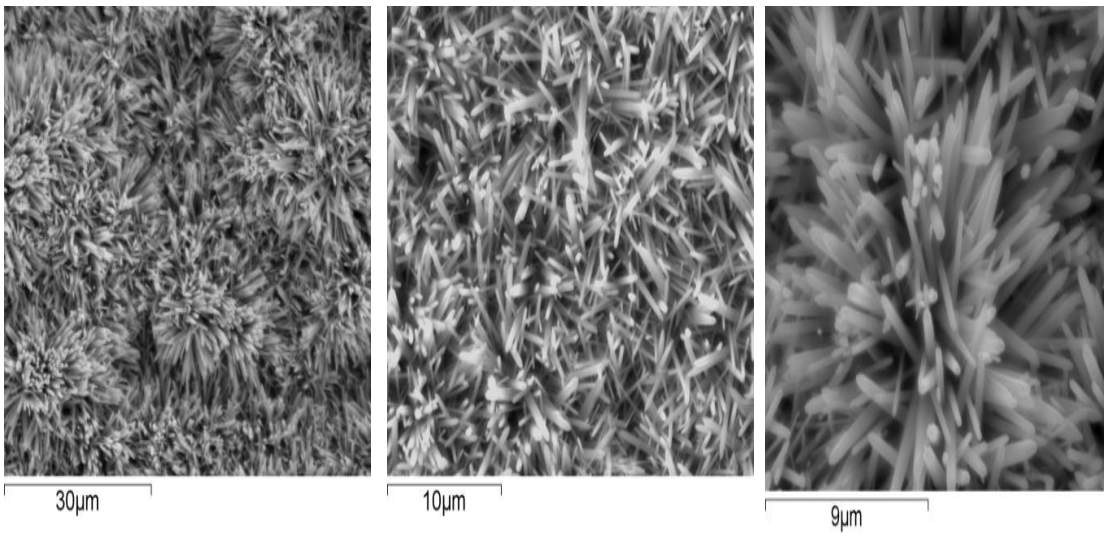

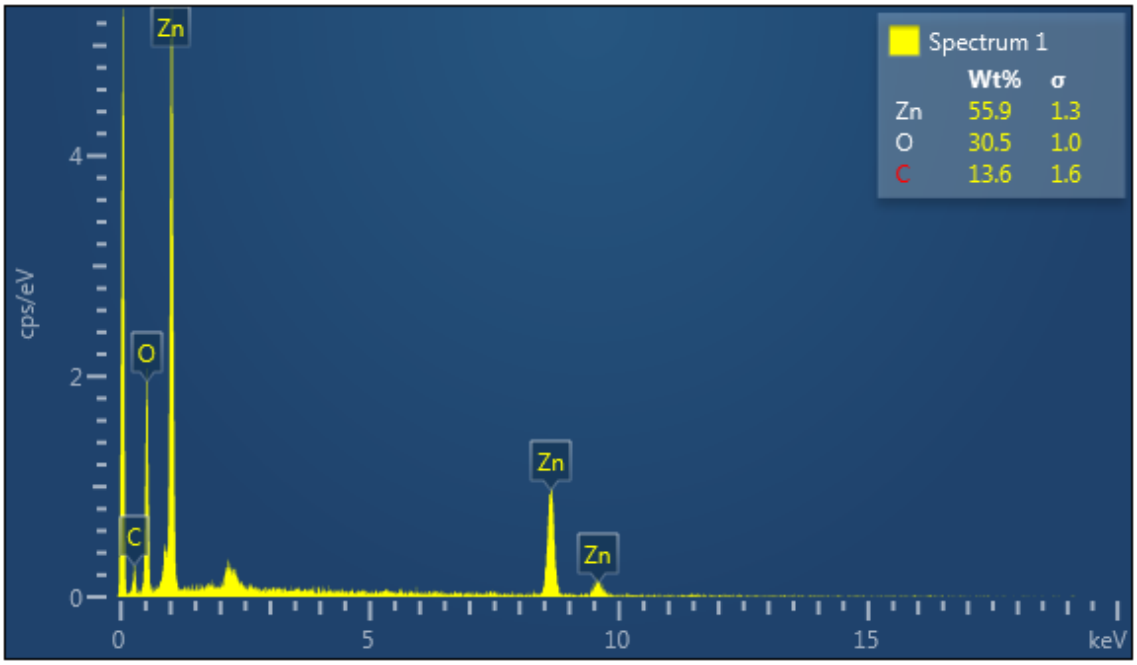

Figure 4-3 SEM images and EDX analysis of ZnO/MoS2

4.2 X-Ray Diffraction

The x-ray diffraction (XRD) studies were accomplished by using CuKα radiations (λ=0.14056nm) to investigate purity and the crystal structure of MoS_2, ZnO and MoS_2/ZnO composite. The powder X-ray pattern of MoS_2, ZnO and MoS_2/ZnO composite has been shown in the Figure 1 given below with reference to JCPDS card No. 65-0160 as MoS_2 and JCPDS card number 79-0205 as ZnO. XRD Pattern of all the samples which are shown in Figure confirms the crystalline nature of MoS_2, ZnO and MoS_2/ZnO composite. It has been observed that peaks of (100), (002), (101), (102), (110), (103), (112) are for ZnO particles while the peaks of (002), (004), (100), (110) assigned for MoS_2 Nanoparticles. MoS_2/ZnO composite XRD showed that peaks of both ZnO as well as MoS_2 resides in the composite which clearly defines its formation. Additionally, the peaks intensity of ZnO has been enhanced which shows the sign of interaction between ZnO and Molybdenum disulphide. The peak at 2Θ=32 ion composite is related to plane (100) as observed for both ingredients While the reflection peak at 58oin composite, resembles to (110) plane. It is evident that the newly made composite has relatively sharper peak at (002) plane and this is an indication of

formation of relatively better crystalline MoS_2 Nanoparticles. As a result, the hexagonal property as well as the crystallinity of the ingredients in the composite is retained.

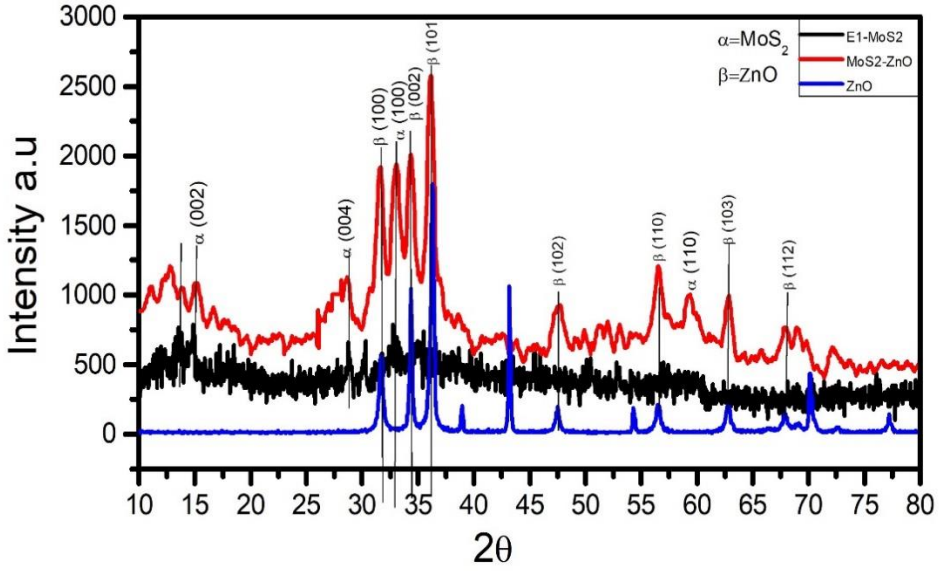

Figure 4-4 XRD of ZnO/ MoS2, ZnO and MoS2

4.3 Raman Spectroscopy

Crystal as well as Structural phases of as prepared ZnO Nano sheets, Molybdenum Nano sheets and their hybrid ZnO/ MoS_2 was examined by Raman spectroscopy as shown in fig---. The as prepared hybrid showed peaks at 323, 435, 570 and 958 cm^{-1}. There is a buldge of MoS_2 at 958 cm^{-1} in the hybrid. The peak between 330-360 cm^{-1} is associated to the molybdenum disulfide vibrational mode. While on the other hand, the peak at 958 cm^{-1} is assigned to the MoS_2 defects, presenting the possibility of molybdenum oxysulfide MoSxOy due to the extremely energetic process in the presence of the zinc granules. The latter can deliver itself oxygen source comprising imperfections developing in the structure of the Nanostructured materials i.e. molybdenum disulfide.

There is anomalous behavior of ZnO at 874 cm^{-1} could be the result of impact created by MoS_2 at their interface. While in ZnO, the peak at 570 cm^{-1} shows the existence of defects. On the other hand, the peaks around 1126 cm^{-1} and 330 cm^{-1} have been observed

due to the multiple phonon scattering process involved in the synthesis of this kind of hybrid.

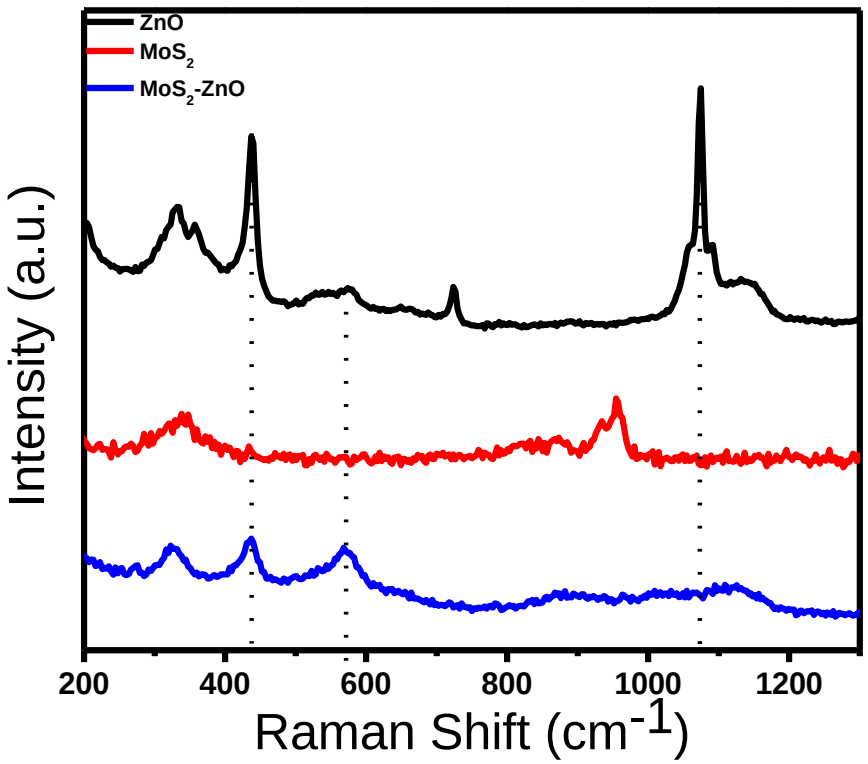

Figure 4-5 Raman Shift of MoS2, ZnO and MoS2/ZnO

4.4 Band-gap calculation

The ZnO sample absorption spectrum corresponds the strong band in the UV region and lighter band in the visible region. However, MoS_2/ZnO Composite shows absorption in both UV region and visible region as the composite includes the ZnO. Figures shows the bandgap evaluation of MoS_2, ZnO and MoS_2/ZnO composite via Tauc plot. MoS_2 shows a direct bandgap of 1.35eV and ZnO show a direct bandgap around 3.23 eV while a direct bandgap of 2.207 eV is observed for MoS_2/ZnO composite. The widening of the MoS_2 band gap in MoS_2/ZnO composite helps in the formation of type-II (staggered) MoS_2/ZnO heterostructure, i.e., the CB of exfoliated MoS_2 was positioned above the CB of ZnO and the VB of ZnO was positioned below the VB of MoS_2. The positioning of

the bands was estimated based on bandgap calculated from UV visible and theoretical work-functions [94]. This kind of arrangement will help in efficient charge carrier separation due to the spatial distribution of bands which seems promising. As the MoS_2 bandgap broaden, it also brings the redox potential in the bandgap region of MoS_2 in the composite which is the main element in achieving the superior photo catalytic performance [94]

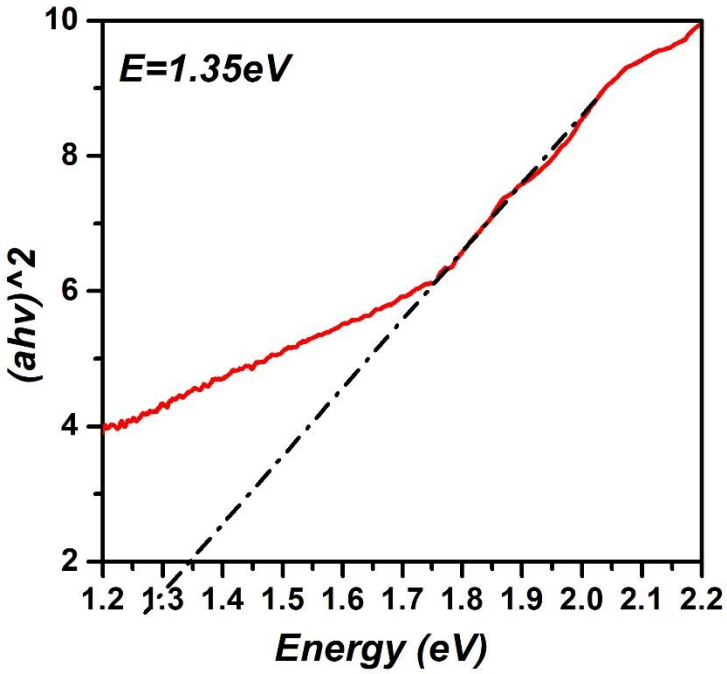

Figure 4-6 Band gap of MoS2

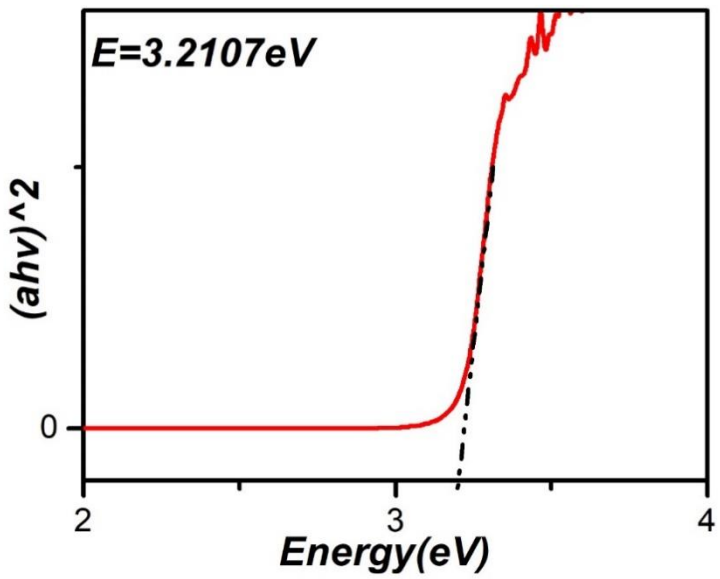

Figure 4-7 Band gap of ZnO

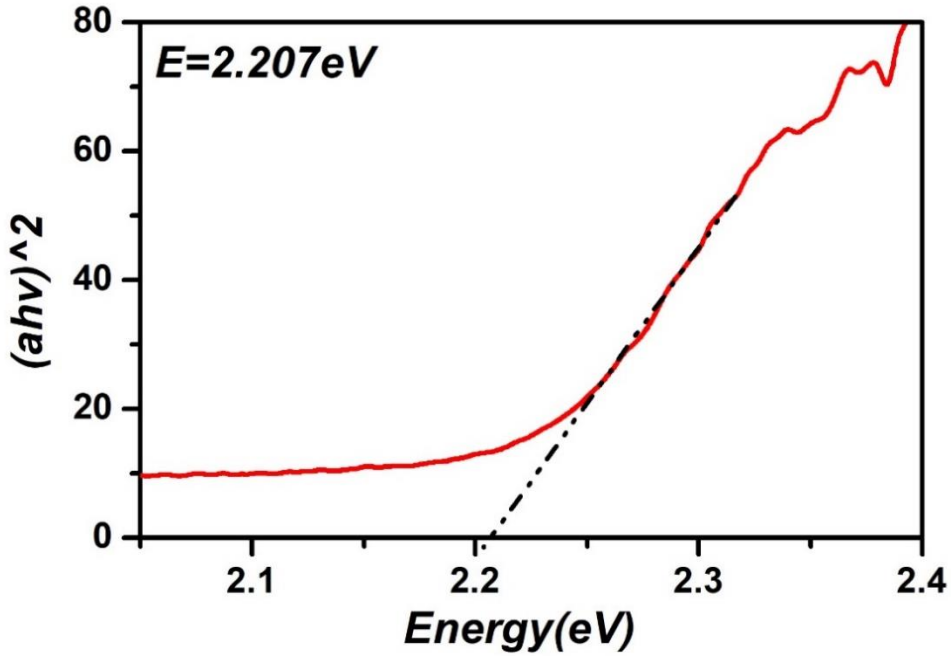

Figure 4-8 Band gap of MoS2/ZnO composite

4.5 Electrochemical measurements

Electrochemical workstation (CHI660E, China) has been used to perform the electrochemical experiments while the temperature is maintained at room temperature. Three electrodes were used during the experiment. A small amount of ZnO, MoS_2 and MoS_2/ZnO were dispersed in Nafion via sonication for 30 minutes. The suspension was then immobilized on glassy carbon electrode (GCE) electrode via drop casting. The fabricated electrodes were referred as ZnO/GCE, MoS_2/GCE and MoS_2/ZnO/GCE and implied as the working electrode for cyclic voltammetry and amperometric measurements where Hg/Hg_2Cl_2 and Pt serves as the reference electrode and counter electrode respectively. The voltage used for Cyclic voltammetry (CV) lies in the potential range +0.8 to -0.5 V at scan rate of 50 mV/s and amperometric response was carried out at -0.35 V in 0.1M PBS (7.0 pH) under the mild stirring.

Electrochemical sensing of glucose

4.6 Cyclic Voltammetry

In order to analyze the sensing ability of the ZnO/GCE, MoS_2/GCE and MoS_2/ZnO/GCE, cyclic voltammograms (CVs) and amperometry response was generated by the ZnO/GCE, MoS_2/GCE and MoS_2/ZnO/GCE and by measuring their electrochemical performance, it will tell the presence of glucose. CV curve obtained in the potential range of +0.8 to -0.5 V at a scan rate of 50 mVs^{-1} used to characterize the electrode.

The normal CV scans of the blank GCE, ZnO/GCE, MoS_2/GCE and MoS_2/ZnO/GCE are shown in Figure 27 The blank GCE electrode showed low current without any definite redox peak. In case of ZnO/GCE, a well-defined pair of redox peaks at -0.3V and 0.25V was observed. These peaks show the increase in the electrochemical activity of the electrode due to ZnO Nanostructure. Immobilizing MoS_2 on GCE shows an oxidation peak at -0.35V along with two reduction peaks at -0.1V and 0.1V. Moreover, an enhancement in the redox peak current value were also observed. On the other way round, a high elevation in the electrode peak current was noticed by incorporating/immobilizing ZnO and MoS_2 together on the surface of GCE. No obvious

change in the redox peak potentials were observed for MoS_2/ZnO/GCE. Such a higher increase on the redox peak current can be allocated to the synergistic effects of both ZnO NPs and MoS_2 as a sensing platform.

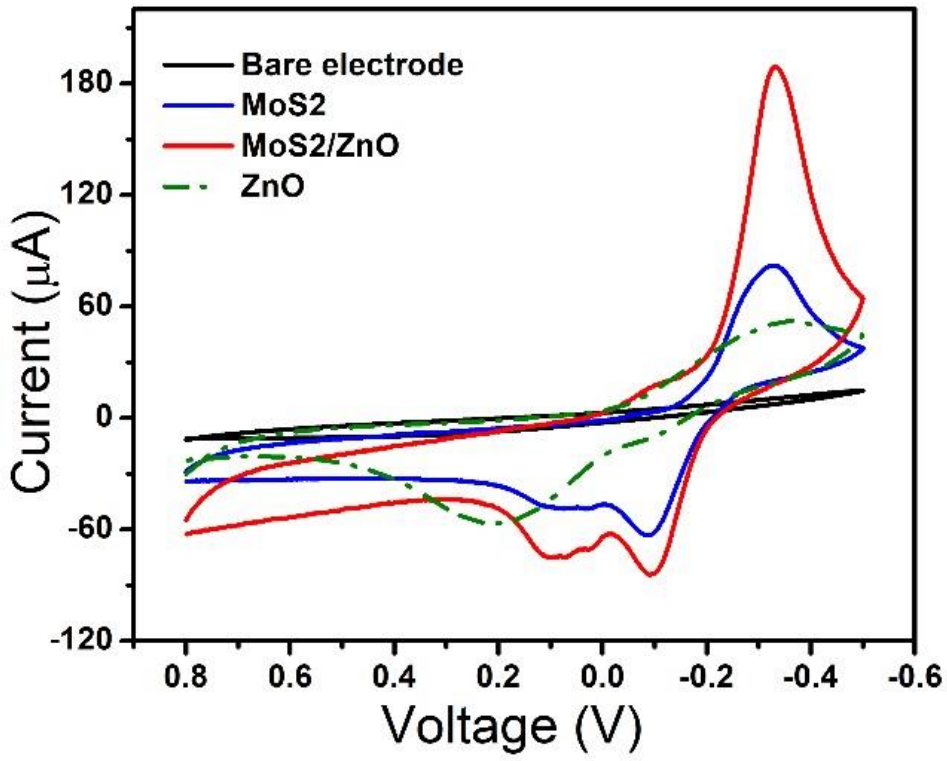

Figure 4-9 CV curve of bare, MoS2 , ZnO and MoS2/ZnO electrode

The MoS_2/ZnO/GCE were further employed for the detection of glucose by adding different glucose concentrations over a range of 10µ to 500µM. A significant increase was observed in the redox peak current by increasing glucose concentration as shown in Figure 28.

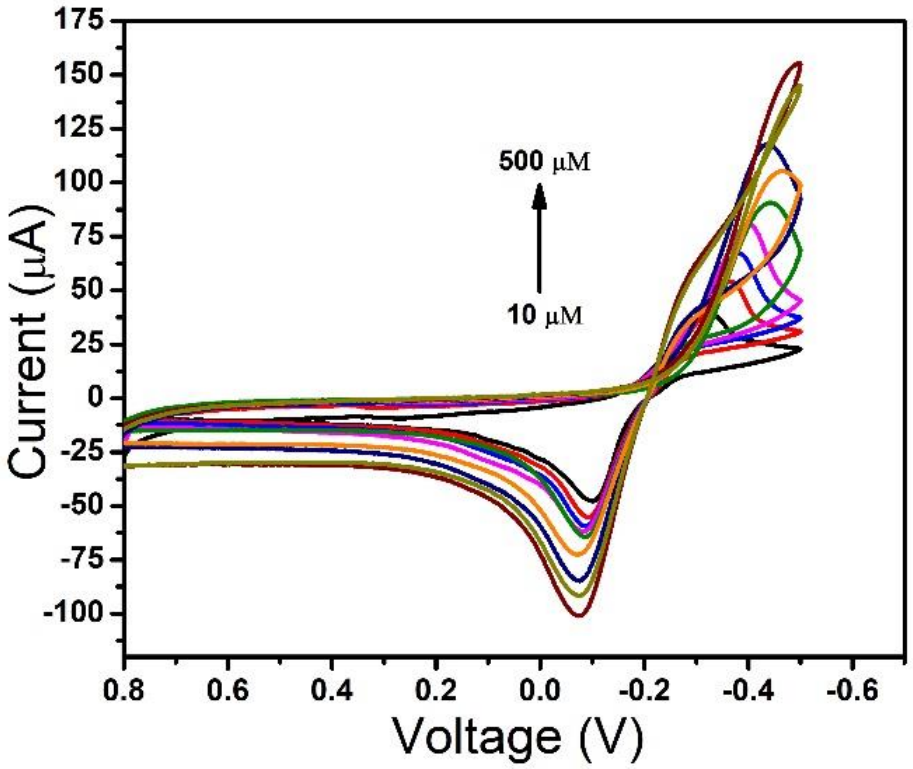

Figure 4-10 CV curve of MoS2/ZnO electrode with glucose

MoS_2/ZnO/GCE was also investigated for their potential scan rate effect on oxidation and reduction peaks current generated by MoS_2/ZnO/GCE in the presence of glucose and shown in Figure 28. As the scan rate increases from 10 mVs^{-1} to 90 mVs^{-1} , oxidation and reduction current also increase for glucose.

The linear fitting of the redox peak current w.r.t scan rate are presented in Figure 29 which shows a linear dependence of the oxidation and reduction peak current over scan rate. This indicates that the glucose is oxidized at the surface of electrode by adsorption-controlled process.

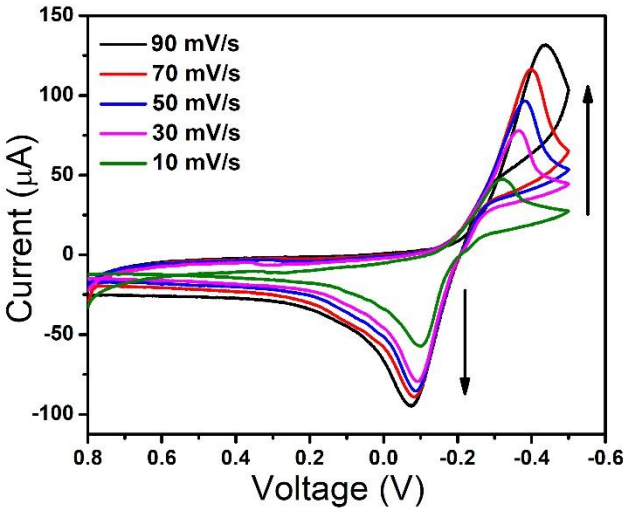

Figure 4-11 CV curves at different scan rates

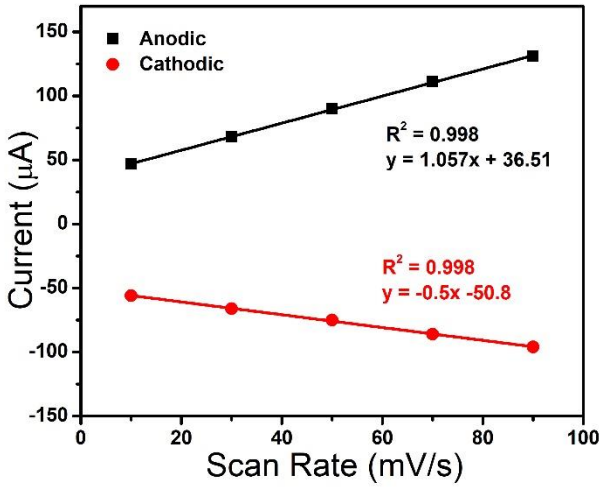

Figure 4-12 Anodic and cathodic linear fitting for sensitivity

The normal amperometric response of the ZnO/GCE, MoS_2/GCE and MoS_2/ZnO/GCE towards the successive addition of several concentrations of glucose at -0.35 V is presented in Figure 31. It can be noticed that the MoS_2/ZnO/GCE showed a quick and sensitive response to the rising concentrations of glucose as compared to the ZnO/GCE and MoS_2/GCE. The response current of the MoS_2/ZnO/GCE is about 3 and 6 times higher than ZnO/GCE and MoS_2/GCE respectively. In addition, 95% steady state

current was also attained by the MoS_2/ZnO/GCE electrode within less than 5 s. This demonstrate the increased electrocatalytic activity and fast electron exchange behavior of the fabricated electrode towards the glucose.

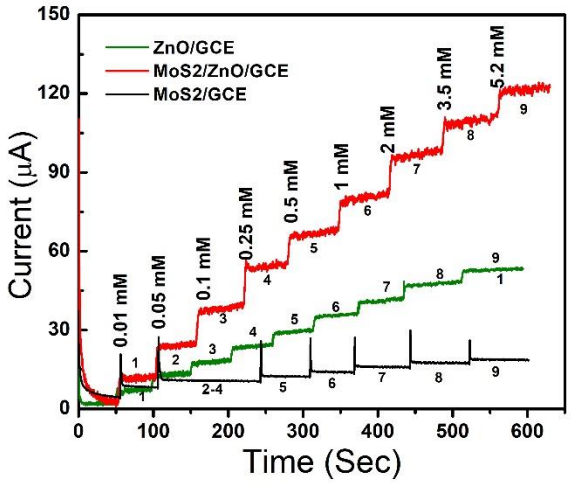

Figure 4-13 Amperometric response of the ZnO/GCE, MoS2/GCE and MoS2/ZnO/GCE towards various concentrations of glucose

Glucose detection has shown through the corresponding calibration plot which is depicted in Figure 31. The response current increases linearly with increasing glucose concentration. The MoS_2/ZnO/GCE electrode provides a sensitivity of 45.121 μA mM^{-1} with a wide linear range (10 μ to 2 mM). The ZnO/GCE and MoS_2/GCE present a sensitivity of 20.929 μA mM^{-1} and 9.854 μA mM^{-1} respectively.

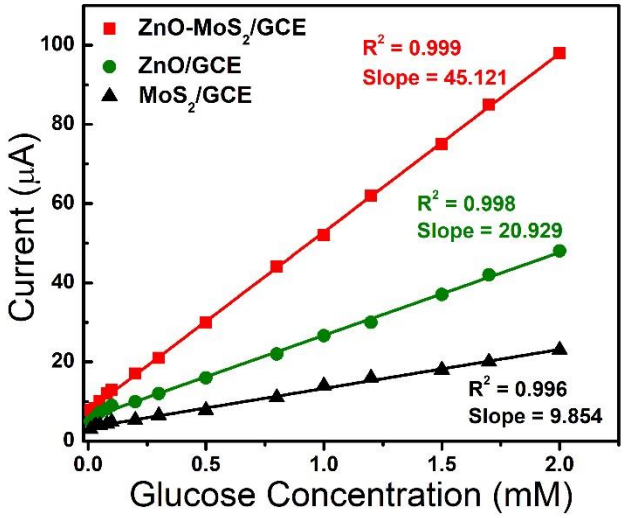

Figure 4-14 Sensitivity of the ZnO/GCE, MoS2/GCE and MoS2/ZnO/GCE towards glucose

In order to determine the LOD , lowest concentration of the glucose was established which showed theelevation in current above the baseline that can be seen reliable and clear.. Figure 33 shows the amperometric response of MoS_2/ZnO/GCE by adding lower concentrations of glucose. The electrode possess a clear and noticeable enhancement in the current generated by adding the glucose as low as 0.025µM which was considered as the low detection limit (LOD) of the biosensor.

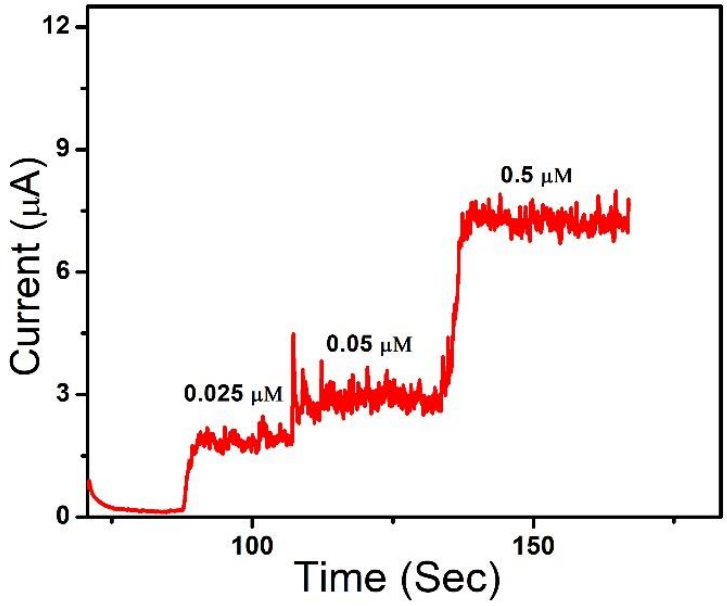

Figure 4-15 Detection limit of MoS2/ZnO/GCE based biosensor for glucose.

Anti-interferences

It is clear that the presence of some electroactive species in serum could affect the biosensor activity, therefore , in order to investigate the anti-interference capability of the biosensor, electroactive species such as L-Cys, urea, cholesterol and AA was added . These species are repeatedly mixed into a constantly agitated 0.1 MPB solution given the potential of -0.8 V possess the scan rate of 50 mV s. The influence of L Cys, urea, cholesterol and AA on the glucose detection at the modified electrode is shown in Figure 34. It is verified from the fig that the cholesterol, urea and L-Cys shows a small increment in current around about 5% which have not any noticeable effect on the biosensor. It is depicted from above results that the constructed biosensor possesses a satisfactory anti-interference ability.

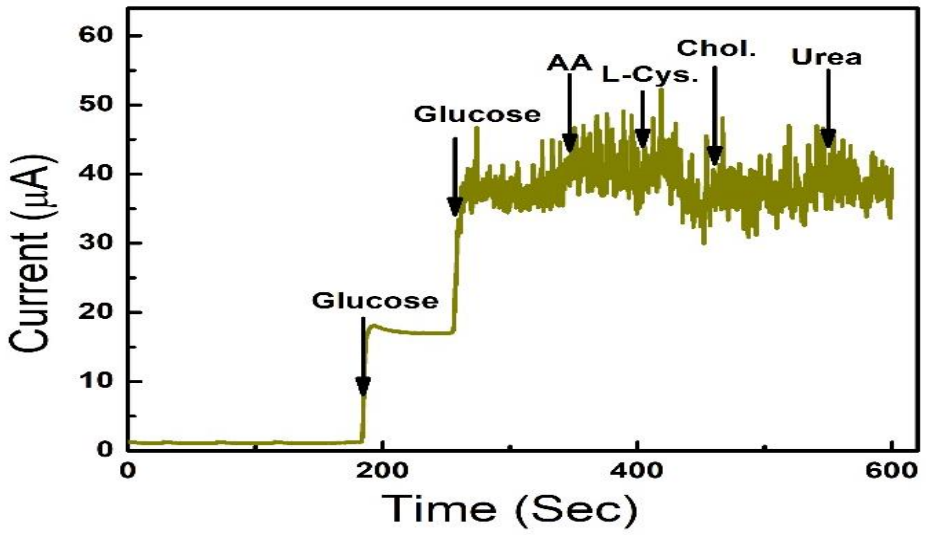

Figure 4-16 Effect of interfering species to the response of the MoS2/ZnO/GCE based biosensor

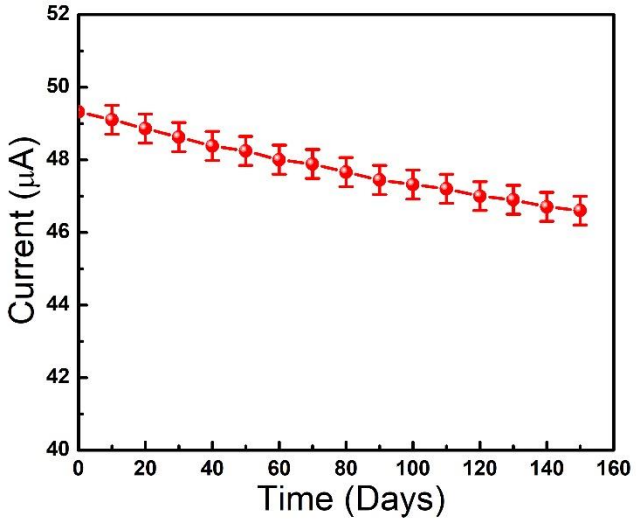

Figure 4-17 Stability of MoS2/ZnO/GCE based biosensor from day 1 to day 150.

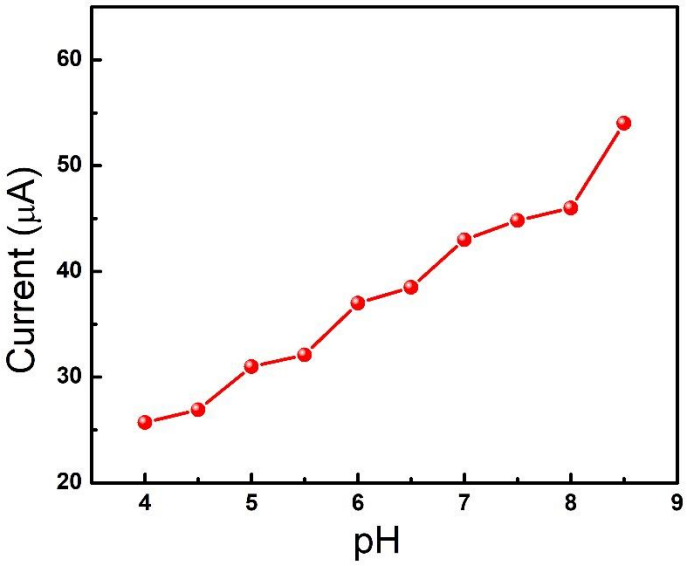

Figure 4-18 Amperometric response of MoS2/ZnO/GCE based biosensor in PB solution with increasing PH from 2 to 8 containing 100uM glucose.

4.7 Photocatalytic degradation of organic dyes

MsO_2/Zn Nanostructures also known for their photocatalytic activity and was assessed for three different organic dyes, methylene blue (MB), rhodamine B (RhB), sandoz turquoise (ST) and sandoz yellow (SY).

4.7.1 Photocatalytic degradation of Methylene Blue

The MB samples were assessed and collected the UV-Vis absorbance spectra from the catalyst reaction mixture at regular interval of time, which is shown in Fig 37. It is appeared that the UV-Vis absorbance maxima of MB decrease with time when reaches to 620 and 675 nm and fade in 22 min. The absence of catalyst during the irradiation did not affect the significant degradation process while in the presence of MsO_2/Zn the photocatalytic reaction is improves and MB degradation completed in just 22 min.

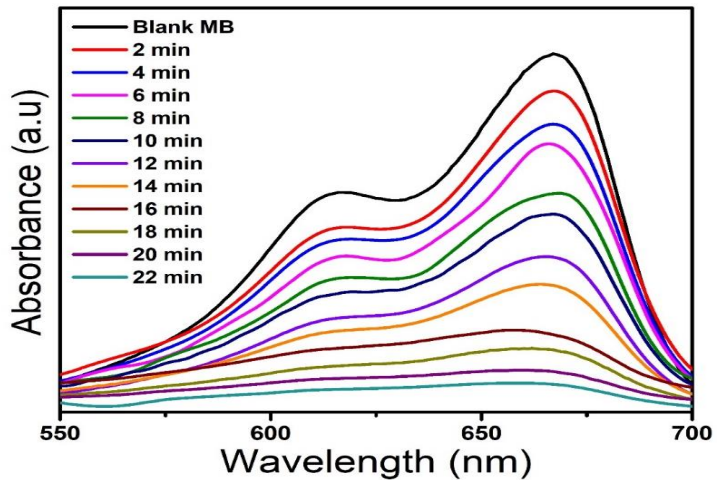

Figure 4-19 Absorbance spectra of MB

4.7.2 Photocatalytic degradation of Rhodamine B

Fig. 38 shows the photocatalytic degradation of RhB which takes place in the presence of MsO_2/Zn of the reaction mixture. It is evident that the MsO_2/ZnO Nanostructures exhibit the quite high photocatalytic activity and the UV-Vis absorbance maxima of RhB at 560 nm fade off with time and disappear in just 45 min. The photocatalytic

reaction is absolutely rapid as compared to the blank reaction as its degradation process of RhB reaches up to ~50% in just 24 min.

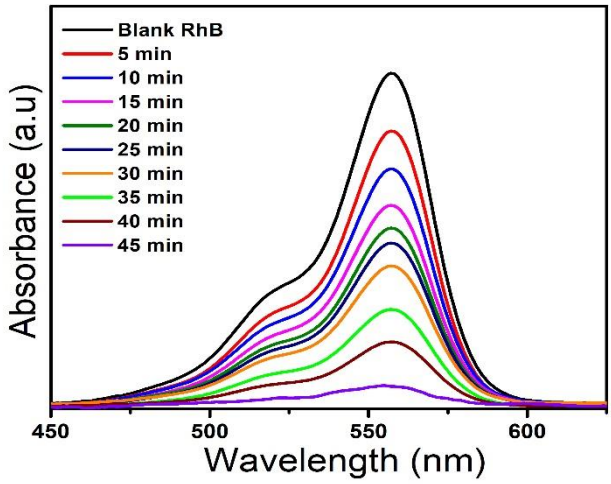

Figure 4-20 Absorbance spectra of RhB

4.7.3 Photocatalytic degradation of Sandoz Turquoise

Fig. 39 shows the photo catalytic degradation of sandoz turquoise (ST) in the presence of reaction mixture of MsO_2/ZnO. It is clear that the MsO_2/Zn Nanostructures exhibit the quite high photocatalytic activity and also showed UV-Vis absorbance maxima of ST at 620 and 690 nm decline with time and disappear in just 24 min. The photocatalytic reaction shows the high activity as compared to the blank reaction by completing the about ~90% ST degradation in just 24 min.

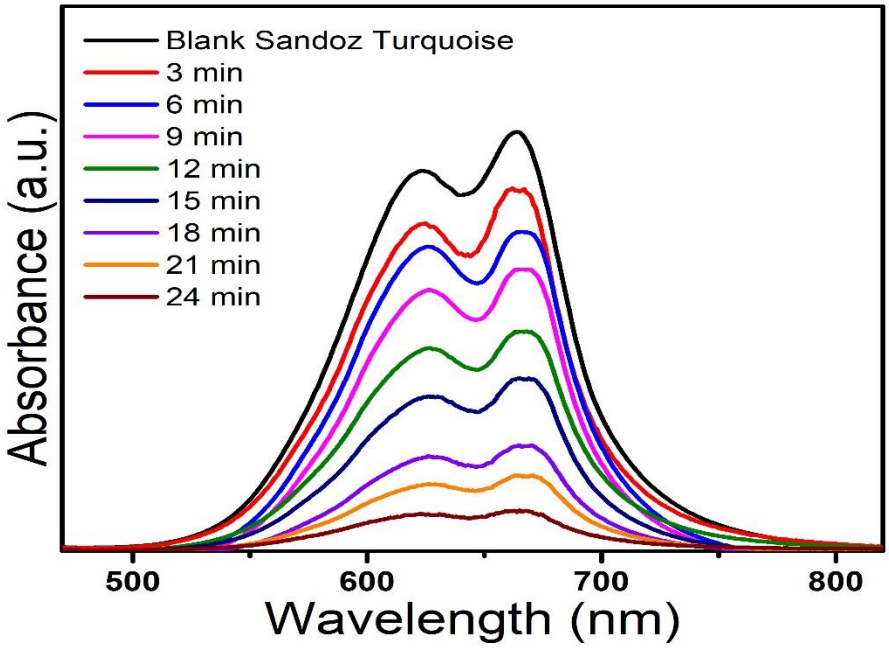

Figure 4-21 Absorbance spectra of sandoz turquoise

4.7.4 Photo-catalytic degradation of Sandoz yellow

Fig. 4.7.5 shows the photo-catalytic degradation of Sandoz yellow (SY) in the presence of MsO_2/Zn of the reaction mixture. it is clear that the photo catalytic activity of the MsO_2/Zn Nanostructures is thoroughly fast and the UV-Vis absorbance maxima of ST at 625 nm decline with time and fade off in just 16 min. The photo catalytic reaction is undoubtly fast when compared to the blank reaction, the degradation of ST reaches up to ~95% in just 16 min (Fig. 3e).

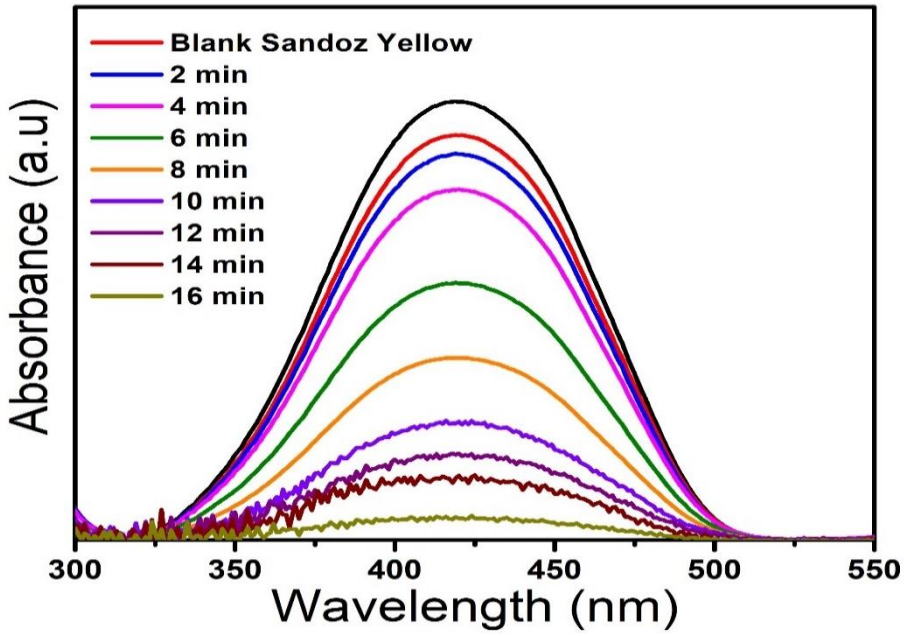

Figure 4-22 Absorbance spectra of sandoz yellow

The photo catalytic degradation of organic dyes under UV illumination were conducted to evaluate the performances of prepared photo catalyst and it is illustrated in figure 41. MB dye solution had about 95% degradation efficiency after 18 min of irradiation, RHB dye solution had about 90% degradation efficiency is 22 min's of irradiation, ST dye solution had about 88% degradation in 24 min's while SY shows only 40% degradation efficiency in 25 min's

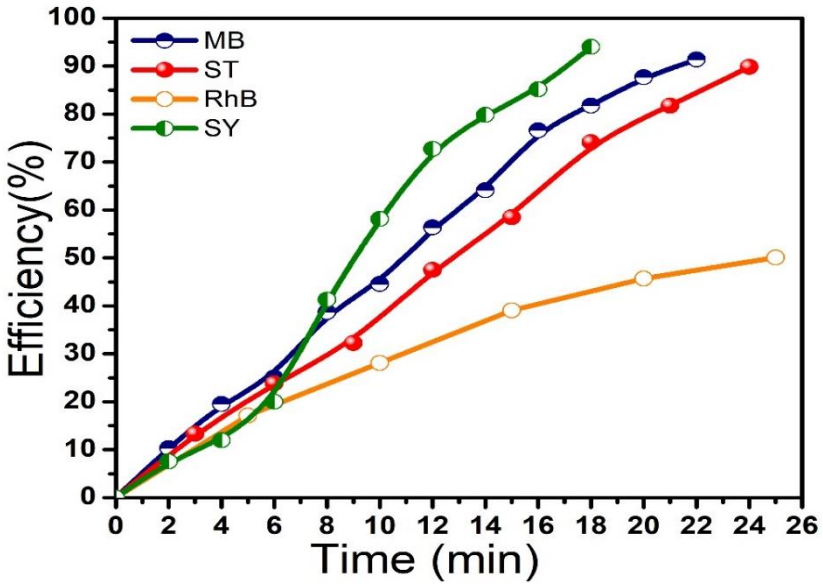

Figure 4-23 Degradation efficiencies of MB, ST ,RhB and SY

Table 1 The characteristics and performance of the produced hybrid nanostructure are compared to biosensors and photo catalysts previously described.

Electrode	**Sensitivity** (μ**A m**$M^{-1}\ cm^{-2}$)	**Linear Range (mM)**	**LOD (µM)**	**Ref**
ZnO nanoparticle	**38.133**	**1–10**	**N/A**	**[96]**
Cu/CuO/ZnO	**408**	**0.1–1**	**18**	**[95]**
ZnO nanowire/EµPAD	**8.24**	**0–15**	**5.95 × 10−2**	**[97]**
C@ZnO/GC	**2.97**	**1–13.8**	**1**	**[98]**
Co3O4 nanofibers	**36.3**	**0. 970uM – 2.04mM**	**0.97**	**[99]**
GOx/Pt-DENs/PAni/CNT/Pt	**42**	**0.001–12**	**0.5**	**[100]**
GOx/PANI/PAN/Pt	**67.1**	**0.002–12**	**2**	**[101]**
MoS2/ZnO	**639.61**	**0.5um-5.5**	**0.025**	**Current work**

Catalyst	**Dye**	**Efficiency (%)**	**Irradiation source**	**Time**	**Ref**
MoS2/ZnO	**MB**	**92**	**UV light**	**21**	**Current work**
MoS2/ZnO	**RHB**	**50**	**UV light**	**24**	**Current work**
MoS2/ZnO	**Sandoz yellow**	**95**	**UV light**	**18**	**Current work**
MoS2/ZnO	**Sandoz Turquoise**	**90**	**UV light**	**23**	**Current work**
Au/Cu2O nanospheres	**mb**	**85**	**UV light**	**120**	**[102]**

Cu@Cu2O nanocomposite	**MB**	**96.5**	**UV light**	**50**	**[103]**
Cu2O/ZnWO	**MB**	**90**	**UV light**	**90**	**[104]**
β-FeSe/g-C3N4	**RHB**	**45**	**UV light**	**180**	**[105]**
g-C3N4 / SAPO-5	**RHB**	**47.15**	**UV light**	**150**	**[106]**
R40-BiFeO3−X	**RHB**	**60**	**UV light**	**360**	**[107]**

Conclusion

In summary, a novel MoS2-ZnO catalyst was successfully synthesized and found to be bifunctional. It has been found that tailoring the band gap and creation of active sites plays a significant impact in increasing catalyst efficiency. A non-enzymatic electrochemical sensor, MoS2-ZnO/GCE-based glucose detection sensor has been discovered to be exceptionally sensitive. enhanced sensitivity of 639.12 μAμM−1 cm−2, Exceptional selectivity and long-term stability. In addition, the sensor also depicit the less sensitivity for the detection limit of 0.025 μM .It has a wide linear range, making it ideal for practical applications. In addition, the binary catalyst is found to be very efficient for the photodegradation of the toxic dyes. The binary catalyst's efficiency has enhanced Because of the change in band gap, Because of the change in band gap, creation of active sites and synergic effects of the MoS2 and ZnO. Hence, these results demonstrate that bifunctional catalyst can be utilized for medical and environmental applications.

References

[1] Microscopy and Histology Catalog, PolysciencesInc, Warrington, PA,18976, 1993-1994.

[2] Shi D.L; N. Itoh N; *Functional Thin Films and Functional Materials: New Concepts and Technologies,*University Press and Springer-Verlag, Berlin,2003.

[3] Committee on Technology, National Science and Technology Council, National Nanotechnology Initiative 2000 Leading to the Next Industrial Revolution, A Report by the Interagency Working Group on Nanoscience, Engineering and Technology

[4] Cao, G;*Nanostructures &Nanomaterials*. London, Imperial College Press,2004.

[5] Binns, C;*Introduction to Nanoscience and Nanotechnology*, HobokenWiley, 2010.

[6] Frederickson, C. J., Koh, J.-Y., & Bush, A. I. (2005). *The neurobiology of zinc in health and disease. Nature Reviews Neuroscience, 6(6), 449–462.*

[7] H.E. Brown, Zinc Oxide: Properties and Applications, International Lead Zinc Research Organization, New York, 1976.

[8] International Zinc Association-Zinc Oxide Information Center, [cited 5/08/2011], Available from: http://www.znoxide.org/index.html.

[9] Klingshirn, C. (2007). *ZnO*: Material, Physics and Applications. ChemPhysChem, 8(6), 782–803.

[10] Özgür, Ü., Alivov, Y. I., Liu, C., Teke, A., Reshchikov, M. A., Doğan, S., … Morkoç, H. (2005). *A comprehensive review of ZnO materials and devices. Journal of Applied Physics, 98(4), 041301.*

[11] G. Auer, W.D. Griebler, B. Jahn, Industrial Inorganic Pigments, 3rd ed., Wiley-VCH Verlag GmbH & Co. KGaA, Weinheim, 2005.

[12] Patnaik P, Handbook of Inorganic Chemicals, McGraw Hill, New York, 2003.

[13] Umicore, EU Classification-Directive 67/548/EEC, [cited 22/10/2010], Avilable

from:http://www.zincchemicals.umicore.com/zcProducts/fineZincPowders/EHS/classification.htm.

[14] Regulation (EC) No 1272/2008 of the European Parliament and of the Council of 16 December 2008 on classification, labelling and packaging of substances and mixtures, amending and repealing Directives 67/548/EEC and 999/45/EC, and amending Regulation (EC) No 1907/2006, OJEU, 51 (2008).

[15] Heideman G, Noordermeer J, Datta W.M.R, Baarle N.B.v, Various ways to reduce zinc oxide levels in S-SBR rubber compounds, Macromol. Symp. 245–246 (2006) 657–667.

[16] Mortimer M, Kasemets K, Kahru A, Toxicity of ZnO and CuO Nanoparticles to ciliated protozoa Tetrahymena thermophila, Toxicology 269 (2010) 182–189.

[17] Nohynek G.J, Lademann J, Ribaud C, Roberts M.S, Grey goo on the skin? Nanotechnology, cosmetic and sunscreen safety, Crit. Rev. Toxicol. 37 (2007)251–277.

[18] Burnett M.E, Wang S.Q, Current sunscreen controversies: a critical review, Photodermatol. Photoimmunol. Photomed. 27 (2011) 58–67.

[19] ASTM Standards, Standard classification for rubber compounding materials—zinc oxide (D 4295-89), 2005.

[20] Wang T.X, Lou T.J, Solvothermal synthesis and photoluminescence properties of ZnO Nanorods and Nanorod assemblies from ZnO2 Nanoparticles, Mater. Lett. 62 (2008) 2329–2331.

[21] Wang Z.L., Nanostructures of zinc oxide, Mater. Today 7 (2004) 26–33.

[22] S. Mahmud, M. Johar Abdullah, M.Z. Zakaria, Nanoscopic inhomogeneity in French process for large scale manufacturing of zinc oxide, Proc. IMFP (2005).

[23] Jang J.S, Yu C.-J, Choi S.H, Ji S.M, Kim E.S, Lee J.S, Topotactic synthesis of mesoporous ZnS and ZnO Nanoplates and their photocatalytic activity, J. Catal. 254 (2008) 144–155.

[24] Kakiuchi K, Hosono E, Kimura T, Imai H, Fujihara S, Fabrication of mesoporous ZnO Nanosheets from precursor templates grown in aqueous solutions, J. Sol-Gel Sci. Technol. 39 (2006) 63–72.

[25] Mahmud S, Abdullah M.J, Nanotripods of zinc oxide, IEEE Conf. Emerging Technol.—Nanoelectron. (2006) 442–446.

[26] Shen L, Zhang H, Guo S, Control on the morphologies of tetrapod ZnO Nanocrystals, Mater. Chem. Phys. 114 (2009) 580–583.

[27] Ding Y, Wang Z.L, Structures of planar defects in ZnO Nanobelts and Nanowires, Micron 40 (2009) 335–342.

[28] Wang Z.L, Zinc oxide Nanostructures: growth, properties and applications, J. Phys.: Condens. Matter 16 (2004) R829–R858.

[29] Yu W, Pan C, Low temperature thermal oxidation synthesis of ZnO Nanoneedles and the growth mechanism, Mater. Chem. Phys. 115 (2009) 74–79.

[30] Ashfold M.N.R, Doherty R.P, Angwafor N.G, Riley D.J, Sun Y, The kinetics of the hydrothermal growth of ZnO Nanostructures, Thin Solid Films 515 (2007) 8679–8683.

[31] Moezzi A, Cortie M, McDonagh A, Aqueous pathways for the formation of zinc oxide Nanoparticles, Dalton Trans. 40 (2011) 4871–4878.

[32] Walde G, Rudy A, Oxyde de zinc, carbonate de zinc et carbonate de zinc basique, leur procédé de fabrication et leur utilisation, French Patent FR2641268 (1990).

[33] Look D.C, Claflin B, P-type doping and devices based on ZnO, Phys. Status Solidi B 241 (2004) 624–630.

[34] Mao F, Deng H, Dai L, Chen J, Yuan Z, Li Y, High quality p-type ZnO film growth by a simple method and its properties, Chin. Sci. Bull. 53 (2008) 2582–2585.

[35] Kawasaki M, Ohtomo A, Fukumura T, Tsukazaki A, Ohtani M, Method of manufacturing thin film, method of manufacturing P-type zinc oxide thin film and semiconductor device, U.S. Patent 20080118769 (2008).

[36] Jacobs K, Schulz D, Klimm D, Ganschow S, Melt growth of ZnO bulk crystals in Ir crucibles, Solid State Sci. 12 (2010) 307–310.

[37] Schulz D, Ganschow S, Klimm D, Struve K, Inductively heated Bridgman method for the growth of zinc oxide single crystals, J. Cryst. Growth 310 (2008) 1832–1835

[38] Schulz D, Ganschow S, Klimm D, Neubert M, Roßberg M, Schmidbauer M, Fornari R, Bridgman-grown zinc oxide single crystals, J. Cryst. Growth 296 (2006) 27–30.

[39] Look D.C, Reynolds D.C, Sizelove J.R, Jones R.L, Litton C.W, Cantwell G, W.C. Harsch, Electrical properties of bulk ZnO, Solid State Commun. 105 (1998) 399–401.

[40] Springer Handbook of Electronic and Photonic Materials, Springer, 2006.

[41] Hsu H.-C, Wu C.-Y, Cheng H.-M, Hsieh W.-F, Band gap engineering and stimulated emission of ZnMgO Nanowires, Appl. Phys. Lett., 89 (2006) 013101/013101–013101/013103.

[42] Karpina V.A, Lazorenko V.I, Lashkarev C.V, Dobrowolski V.D, Kopylova L.I, Baturin V.A, Pustovoytov S.A, Karpenko A.J, Eremin S.A, Lytvyn P.M, Ovsyannikov V.P, Mazurenko E.A, Zinc oxide—analogue of GaN with new perspective possibilities, Cryst. Res. Technol. 39 (2004) 980–992.

[43] Klingshirn C, Hauschild R, Fallert J, Kalt H, Room-temperature stimulated emission of ZnO: Alternatives to excitonic lasing, Phys. Rev. B: Condens. Matter, 75 (2007) 115203/115201–115203/115209.

[44] Li Y.Y, Li Y.X, Wu Y.L, Sun W.L, Preparation and photoluminescent properties of zinc oxide phosphor, J. Lumin. 126 (2007) 177–181.

[45] Lin C.H, Chiou B.-S, Chang C.H, Lin J.D, Preparation and cathodoluminescence of ZnO phosphor, Mater. Chem. Phys. 77 (2003) 647–654.

[46] Hirschwald W.H, Zinc oxide: an outstanding example of a binary compound semiconductor, Acc. Chem. Res. 18 (1985) 228–234.

[47] Guilmeau E, Maignan A, Martin C, Thermoelectric oxides: effect of doping in delafossites and zinc oxide, J. Electron. Mater. 38 (2009) 1104–1108.

[48] Cheng H, Xu X.J, Hng H.H, Ma J, Characterization of Al-doped ZnO thermoelectric materials prepared by RF plasma powder processing and hot press sintering, Ceram. Int. 35 (2009) 3067–3072.

[49] Klingshirn, C. (2007). *ZnO*: Material, Physics and Applications. ChemPhysChem, 8(6), 782–803.

[50] Ellmer K., Klein A., Rech B., Transparent Conductive Zinc Oxide, Springer, New York, 2008.

[51] N. Sano, H. Wang, M. Chowalla, I. Alexandrou, G. A. J Amaratunga, M. Natio, T. Kanki, "Fabrication of In-Organic Molybdenum Disulfide Fullerenes by Arc in Water", Chem. Phys.Lett, **368** (2003) 331-337.

[52] Zach, M. P., Inazu, K., Ng, K. H., Hemminger, J. C., & Penner, R. M. (2002). *Synthesis of Molybdenum Nanowires with Millimeter-Scale Lengths Using Electrochemical Step Edge Decoration. Chemistry of Materials, 14(7), 3206–3216.*

[53] J. Kibsgaard, Z. B Chen, B.N. Reinecke, T. F. Jaramillo, "Nat.Matter", **11** (2012)963-969.

[54] Wang, F., Li, G., Zheng, J., Ma, J., Yang, C., & Wang, Q. (2018). *Hydrothermal synthesis of flower-like molybdenum disulfide microspheres and their application in electrochemical supercapacitors. RSC Advances, 8(68), 38945–38954.*

[55] Andersson, M., Österlund, L., Ljungström, S., & Palmqvist, A. (2002). *Preparation of Nanosize Anatase and Rutile TiO2by Hydrothermal Treatment of Microemulsions and Their Activity for Photocatalytic Wet Oxidation of Phenol. The Journal of Physical Chemistry B, 106(41), 10674–10679.*

[56] Lowe C. R. "Biosensors.", Trends in Biotechnology. **2(3)** (1984), 59-65.

[57] Chaubey A, Malhotra B.D, "Mediated Biosensors," Bioelectronics & Bioelectronics, **17(6-7)** (2002)441-456.

[58] Norberto Masciocchi, "Data collection: Experimental set-ups and Sample Preparation, International Workshop on Structural Determination from Powder Diffraction Data," Villigen (CH), June 18-22, 2008.

[59] Ando, J., Yano, T., Fujita, K., & Kawata, S. (2013). *Metal Nanoparticles for Nano-imaging and Nano-analysis. Physical Chemistry Chemical Physics, 15(33), 13713.*

[60] Mak, K. F., Lee, C., Hone, J., Shan, J., & Heinz, T. F. (2010). *Atomically ThinMoS2: A New Direct-Gap Semiconductor. Physical Review Letters, 105(13).*

[61] Yi-Hsien Lee, Xin-Quan Zhang, Wenjing Zhang, Mu-Tung Chang, Cheng-Te Lin, Kai-Di Chang, Ya-Chu Yu, Jacob Tse-Wei Wang, Chia-Seng Chang, Lain-Jong Li and Tsung-Wu Lin, "Synthesis of Large-Area MoS2 Atomic Layers with Chemical Vapor Deposition", Institute of Atomic and Molecular Sciences, Academia Sinica, 2013.

[62] Biju, V., Itoh, T., & Ishikawa, M. (2010). *Delivering quantum dots to cells: bioconjugated quantum dots for targeted and nonspecific extracellular and intracellular imaging. Chemical Society Reviews, 39(8), 3031.*

[63] Li, X.-L., & Li, Y.-D. (2004). *MoS2Nanostructures: Synthesis and Electrochemical Mg2+Intercalation. The Journal of Physical Chemistry B, 108(37), 13893–13900.*

[64] Binnig, G., & Rohrer, H. (1983). *Scanning tunneling microscopy. Surface Science, 126(1-3), 236–244.*

[65] Bogner A, Thollet G, Basset D, Jouneau PH, Gauthier C, "Wet STEM: A New Development in Environmental SEM for Imaging Nano-Objects Included in a Liquid Phase", Ultra microscopy, **104** (2005), 290–301.

[66] Chen, Y., Zou, C., Mastalerz, M., Hu, S., Gasaway, C., & Tao, X. (2015). *Applications of Micro-Fourier Transform Infrared Spectroscopy (FTIR) in the Geological Sciences—A Review. International Journal of Molecular Sciences, 16(12), 30223–30250.*

[67] A. Hazra, B. Bhowmik, K. Dutta, V. Manjuladevi, R. K. Gupta, P. Bhattacharyya, "Low Temperature Methanol Sensing by p type Nano Titania: Correlation with Defects States and Schottky Barrier Model", IEEE Transactions on Nanotechnology (IEEE), 14(2015)187-195.

[68] Connes, J. Connes, "Near-Infrared Planetary Spectra by Fourier Spectroscopy. I. Instruments and Results", Journal of the Optical Society of America, **56** (1966), 896– 910.

[69] Smith, D. R. Morgan, R. L. Loewenstein, E.V. (1968). "Comparison of the Radiance of Far-Infrared Sources". J. Opt. Soc. Am. **58** (3) (1968), 433–434.

[70] Chamberain, J. Gibbs, J. E. Gebbie, H.E, "The Determination of Refractive Index Spectra by Fourier Spectrometry", Infrared Physics, **9 (4)** (1969), 189–209.

[71] Urabe, H. Tominaga, Y. Kubota, K. (1983). "Experimental Evidence of Collective Vibrations in DNA Double Helix Raman Spectroscopy", Journal of Chemical Physics. **78** (10) (1983): 5937-5939.

[72] Gardiner, D. J. (1989), "Practical Raman Spectroscopy", Springer-Verlag. ISBN, (1989), 978-0-387-50254.

[73] Iliev, M. N. Abrashev, M. V. Laverdiere, J. Jandi, S. et al. "Distortion-Dependent Raman Spectra and Mode Mixing in RMnO3 Perovskites (R=La, Pr, Nd, Sm, Eu, Gd, Tb, Dy, Ho, Y)", "Physical Review B", (February 16, 2006).

[74] Schlücker, S. et al, "Design and Synthesis of Raman Reporter Molecules for Tissue Imaging by Immuno-SERS Microscopy", Journal of Biophotonics. **4(6)**(2011): 453– 463.

[75] Howell G. M. Edwards, John M. Chalmers, "Raman Spectroscopy in Archaeology and Art History", Royal Society of Chemistry, 2005.

[76] Ben Vogel, "Raman Spectroscopy Portends Well for Standoff Explosives Detection", Jane's, 2008.

[77] Skoog, Douglas A. Holler, F. James Crouch, Stanley R, "Principles of Instrumental Analysis", Belmont, CA: Thomson Brooks, ISBN 2016, 169-173.

[78] Metha, Akul, Misra, Prabhakar Dubinskii, Mark, "Limitations and Deviations of BeerLambert Law", Ultraviolet Spectroscopy and UV Lasers. New York: Marcel Dekker, **4** (14 May 2012), 8247-0668.

[79] Tanyuan Wang, Haichuan Zhu, Junqiao Zhuo, Zhiwei Zhu, Pagona Papakonstantinou, Gennady Lubarsky, Jian Lin and Meixian Li, "Biosensor Based on Ultrasmall MoS2 Nanoparticles for Electrochemical Detection of H2O2 Released by Cells at the Nanomolar Level", Anal. Chem. **85**(2013), 10289-10295.

[80] Tharangattu N Narayanan, Chiranjeevi S R Vusa and Subbiah Alwarappan, Selective and efficient electrochemical biosensing of ultrathin molybdenum disulfide sheets, Nanotechnology **25** (2014) 335702.

[81] J. Wang, Electrochemical glucose biosensors, Chem. Rev. 108 (2008) 814X. Niu, M. Lan, H. Zhao, C. Chen, Highly Sensitive and Selective Nonenzymatic Detection of Glucose Using Three-Dimensional Porous Nickel Nanostructures, Anal. Chem. 85 (2013) 3561.

[82] R.Wilson,A.P.F. Turner, Glucose oxidase: an ideal enzyme, Biosens. Bioelectron. 7 (1992) 165

[83] J. Wang, Glucose Biosensors: 40 Years of Advances and Challenges, Electroanal. 13 (2001) 983

[84] X. Niu, M. Lan, H. Zhao, C. Chen, Well-Dispersed Pt Cubes on Porous Cu Foam: High-Performance Catalysts for the Electrochemical Oxidation of Glucose in Neutral Media, Chem. -Eur. J. 19 (2013) 9534.

[85] J. Song, L. Xu, R. Xing, W. Qin, Q. Dai, H. Song, Ag Nanoparticles coated NiO Nanowires hierarchical Nanocomposites electrode for nonenzymatic glucose biosensing, Sensor Actuat. B:chem 182 (2013) 675

[86] S.Wang, Y. Boyjoo, A. Choueib, Z.H. Zhu, Removal of dyes from aqueous solution using fly ash and red mud, Water Res. 39 (2005) 129–138.

[87] M.A.M. Khraisheh, M.A. Al-Ghouti, S.J. Allen, M.N. Ahmad, Effect of OH and silanol groups in the removal of dyes from aqueous solution using diatomite, Water Res. 39 (2005) 922–932

[88] Q. Sun, L. Yang, The adsorption of basic dyes from aqueous solution on modified peat–resin particle, Water Res. 37 (2003) 1535–1544.

[89] J.H. Sun, S.P. Sun, G.L. Wang, L.P. Qiao, Degradation of azo dye Amido black 10B in aqueous solution by Fenton oxidation process, Dyes Pigments 74 (2007) 647–652.

[90] M.A. Behnajady, N. Modirshahla, N. Daneshvar, M. Rabbani, Photocatalytic degradation of CI Acid Red 27 by immobilized ZnO on glass plates in continuousmode, J. Hazard. Mater. 140 (2007) 257–263

[91] A. Akyol, M. Bayramoglu, The degradation of an azo dye in a batch slurry photocatalytic reactor, Chem. Eng. Proc. 47 (2008) 2150–2156.

[92] S. Anandan, A. Vinu, T. Mori, N. Gokulakrishnan, P. Srinivasu, V. Murugesan, K. Ariga, Photocatalytic degradation of 2, 4, 6-trichlorophenol using

lanthanum doped ZnO in aqueous suspension, Catal. Commun. 8 (2007) 1377–1382

[93] J.G. Yu, X.X. Yu, Hydrothermal Synthesis and Photocatalytic Activity of Zinc Oxide Hollow Spheres, Environ. Sci. Technol. 42 (2008) 4902–4907.

[94] S.S. Lo, T. Mirkovic, C.H. Chuang, et al., Adv. Mater. 23 (2011) 180–197.

[95] S. SoYoon, A. Ramadoss, B. Saravanakumar, S.J. Kim, Novel Cu/CuO/ZnO hybrid hierarchical nanostructures for non-enzymatic glucose sensor application, J. Electroanal. Chem. 717 (2014) 90–95

[96] Singh, K.; Umar, A.; Kumar, A.; Chaudhary, G.R.; Singh, S.; Mehta, S.K. Non-enzymatic glucose sensor based on well-crystallized ZnO nanoparticles. Sci. Adv. Mater. 2012, 4, 994–1000.

[97] Li, X.; Zhao, C.; Liu, X.Y. A paper-based microfluidic biosensor integrating zinc oxide nanowires for electrochemical glucose detection. Microsyst. Nanoeng. 2015, 1, 15014.

[98] Non-Enzymatic Glucose Sensor Composed of Carbon-Coated Nano-Zinc Oxide

[99] Y. Ding, Y. Wang, L. Su, H. Zhang, Y. Lei, J. Mater. Chem. 2010, 20, 9918.

[100] Xu, L.; Zhu, Y.; Yang, X.; Li, C. Amperometric biosensor based on carbon nanotubes coated with polyaniline/dendrimer-encapsulated Pt nanoparticles for glucose detection. Mater. Sci. Eng. C 2009, 29, 1306–1310.

[101] Xue, H.; Shen, Z.; Li, C. Improved selectivity and stability of glucose biosensor based on in situ electropolymerized polyaniline-polyacrylonitrile composite film. Biosens. Bioelectron. 2005, 20, 2330–2334

[102] Y. Shang, Acta Phys.-Chim. Sin., 2013, 29(8), 1819–1826.

[103] L. Xu, C. Srinivasakannan, J. Peng, M. Yan, D. Zhang and L. Zhang, Appl. Surf. Sci., 2015, 331, 449–454.

[104] L. Tian, Y. Rui, K. Sun, W. Cui and W. An, Nanomaterials, 2018, 8, 33.

[105] Shen, S.; Zhong, W.; Wang, Z.G.; Lin, Z.; Feng, S. β-FeSe nanorods composited g-C3N4 with enhanced photocatalytic efficiency. R. Soc. Open Sci. 2019, 6, 181886

[106] Qiu, L.; Zhou, Z.; Qiu, X.; Duo, S. Synthesis and photocatalytic degradation performance of g-C3N4 /CQDs/ SAPO-5 ternary composite. Key Eng. Mater. 2018, 768, 201–205.

[107] Di, L.; Yang, H.; Xian, T.; Chen, X. Enhanced photocatalytic activity of NaBH4 reduced BiFeO3 nanoparticles for rhodamine B decolorization. Materials 2017, 10, 1118.